Computers and Electronics in Agriculture 216 (2024) 108523

Contents lists available at ScienceDirect

Computers and Electronics in Agriculture

journal homepage: www.elsevier.com/locate/compag

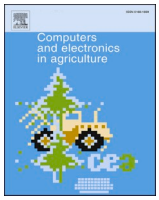

Monthly intercepted photosynthetically active radiation estimation based on the Beer-Lambert's law across the cereal crops of Castilla y León (Spain)

E. Garrachón-Gómez [a], I. García [b], A. García-Rodríguez [a], S. García-Rodríguez [a], C. Alonso-Tristán [a,*]

[a] Research Group Solar and Wind Feasibility Technologies, SWIFT. Electromechanical Engineering Department. Avda. Cantabria s/n. 09006 Burgos, Spain
[b] Institute of Smart Cities (ISC), Department of Engineering, Public University of Navarre, Campus Arrosadía, 31006 Pamplona, Spain

ARTICLE INFO

Keywords:
Cereal crops
GIS
fIPAR
PAR
IPAR

ABSTRACT

Agriculture is by far the most important economic activity in the Spanish autonomous region of Castilla y León. Numerous factors influence crop development but one of the most related variables to the photosynthetic process is Photosynthetically Active Radiation (*PAR*). Estimating Intercepted Photosynthetically Active Radiation (*IPAR*) in different crops through the Beer-Lambert law could be a relevant factor in crop season planning by enabling photosynthesis monitoring. The Beer-Lambert Law is applied in this study to the data for almost 2 million hectares of wheat, barley, and maize cultivated in Castilla y León in 2021. The fourteen-year data set of Global Horizontal Irradiance (*GHI*) used to calculate the monthly *PAR* data in the region was collected at 93 meteorological stations (46 in Castilla y León and 47 in neighboring Spanish and Portuguese regions). Two previously published global calibrated models were employed to calculate the *PAR*, with a relative Root Mean Square Error (rRMSE) below 6%, for the measured daily mean values of *PAR* in Burgos. Processing the various NASA Terra and Aqua satellite images yielded the monthly Leaf Area Index (*LAI*) and the literature review provided the light extinction coefficient (*k*). The Geographic Information System (GIS) facilitated visualization of *IPAR* estimates for the three cereal crops in all months of its growing season. Wheat and barley reach their *IPAR* peaks in June and July, while maize peaks in July and August. In addition, the fraction of Intercepted Photosynthetically Active Radiation (*fIPAR*) was calculated in different provinces to assess *PAR* interception for each cereal at different growing stages. In June, almost 50% of the wheat area in Burgos, Palencia and Soria displayed *fIPAR* values exceeding 45% while in the case of barley only the province of Burgos reached these percentages of area and.*fIPAR*.

1. Introduction

Solar radiation is one of the most relevant variables for the interactions that take place within natural environmental systems, as it is the main source of energy for many biological and physical processes such as evapotranspiration, carbon cycles or plant growth (Wei et al., 2020). The importance of the spatio-temporal distribution of Global Horizontal Irradiance (*GHI*) and Photosynthetically Active Radiation (*PAR*) is linked to the information those indicators provide on crop productivity (Nwokolo and Amadi, 2018), or environmental risk prevention (Jeong et al., 2017).

The use of historical *GHI* data from meteorological and radiometric weather stations in large regions (Benavides Cesar et al., 2023) and their mapping assists with very accurate assessments of solar resource and their behavior. However, data collection at the stations has limitations, due to high operating and maintenance costs, although interpolated surface mapping systems based on a Geographic Information System (GIS) can be used to map large areas at specific spatial and temporal scales (Alsamamra et al., 2009). GIS is one of the tools used in precision agriculture to optimize productivity and to minimize environmental impact (Piccoli et al., 2023). Agriculture is generally the most important economic activity within rural areas and Castilla y León, a region located in the north-west of Spain, is no exception. Approximately one-third of its surface area is arable land where the agricultural sector has always been essential (Consejo Económico y Social de Castilla y León, 2021).

Intercepted Photosynthetically Active Radiation (*IPAR*) is one of the least well-known and yet most influential climatic variables that reflects vegetative development. *IPAR* is usually estimated with the Beer-Lambert Law (Monsi and Saeki, 2005; Zhang et al., 2014).

* Corresponding author.
E-mail address: catristan@ubu.es (C. Alonso-Tristán).

https://doi.org/10.1016/j.compag.2023.108523
Received 3 June 2023; Received in revised form 9 November 2023; Accepted 5 December 2023
Available online 14 December 2023

Nomenclature

CC	Cloud Cover (%)
CIPAR	Cumulative Intercepted Photosynthetically Active Radiation ($MJ \cdot m^{-2}$)
GHI	Global Horizontal Irradiance ($W \cdot m^{-2}$, $MJ \cdot m^{-2}$)
IPAR	Intercepted Photosynthetically Active Radiation ($MJ \cdot m^{-2}$)
fIPAR	Fraction of Intercepted Photosynthetically Active Radiation (%)
k	light extinction coefficient
K_b	direct fraction (dim)
K_d	diffuse fraction (dim)
K_t	clearness index (dim)
LAI	Leaf Area Index ($m^2 \cdot m^{-2}$)
P	pressure (mbar)
PAR	Photosynthetically Active Radiation ($MJ \cdot m^{-2}$)
PPFD	Photosynthetic Photon Flux Density ($\mu mol \cdot m^{-2} \cdot s^{-1}$)
T	air temperature (°C)
T_d	dew point temperature (°C)
Δ	sky brightness (dim)
ε	sky clearness (dim)
θ_Z	solar zenith angle (°)

Abbreviations

GIS	Geographic Information System
MAE	Mean Absolute Error
rMBE	Relative Mean Bias Error
OK	Ordinary Kriging
rRMSE	Relative Root Mean Square Error
UK	Universal Kriging

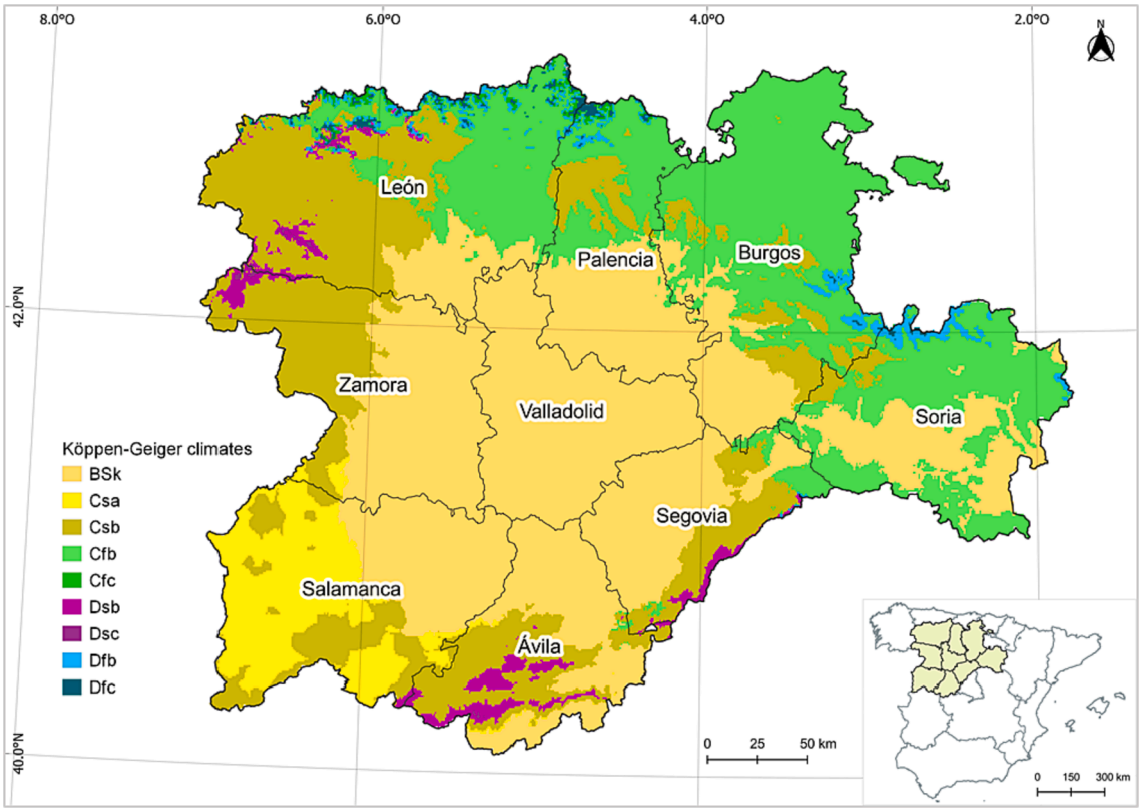

Fig. 1. Climates of the provinces of Castilla y León.

The Beer-Lambert Law is calculated with certain parameters. *PAR* is the component of global solar radiation in the visible spectrum, between 400 and 700 nm. It is a term that could refer to the Photosynthetic Photon Flux Density, *PPFD* ($\mu mol \cdot m^{-2} \cdot s^{-1}$) or to the energy ($W \cdot m^{-2}$) capable of electron transport in the photosynthetic process (Nwokolo and Amadi, 2018). McCree (1972) proposed a constant ratio of 4.57 $\mu mol \cdot J^{-1}$ between *PPFD* and incident *PAR* in terms of energy, to simplify the unit conversion of this parameter. *PAR* is not usually measured, despite its importance as a variable in such varied fields as the agro-food industry or the algae cultivation, so the very few historical databases that exist can only be found at very specific locations. In Spain, a recently developed method using satellite-monitoring data for estimations has been used to determine optimal locations for the installation of *PAR* measurement stations within Spanish territory (Vindel et al., 2018).

Due to this global scarcity of measurements, some authors estimate *PAR* by establishing a constant relationship with Global Horizontal Irradiance (*GHI*), generally between 0.45 and 0.5 (Tsubo and Walker, 2005). However, the ratio is not constant and can vary slightly with location, date, and weather conditions. For instance, Li et al. (2010) studied the monthly mean *PAR*/*GHI* at four different locations and obtained significant differences at two of them. Although this correlation factor yields successful results, there are other ways to obtain *PAR* estimates. One of them is using empirical models, evident in the work of authors since the mid-1990 s up until the present. For instance, Alados et al. (1996) developed multilinear models which use sky clearness (ε) and brightness (Δ) (Perez et al., 1990), solar zenith angle (θ_Z), and dew point temperature (*Td*) as input data, to estimate *PAR*. Yu et al. (2015) developed ten non-linear *PAR* estimation models, using the following

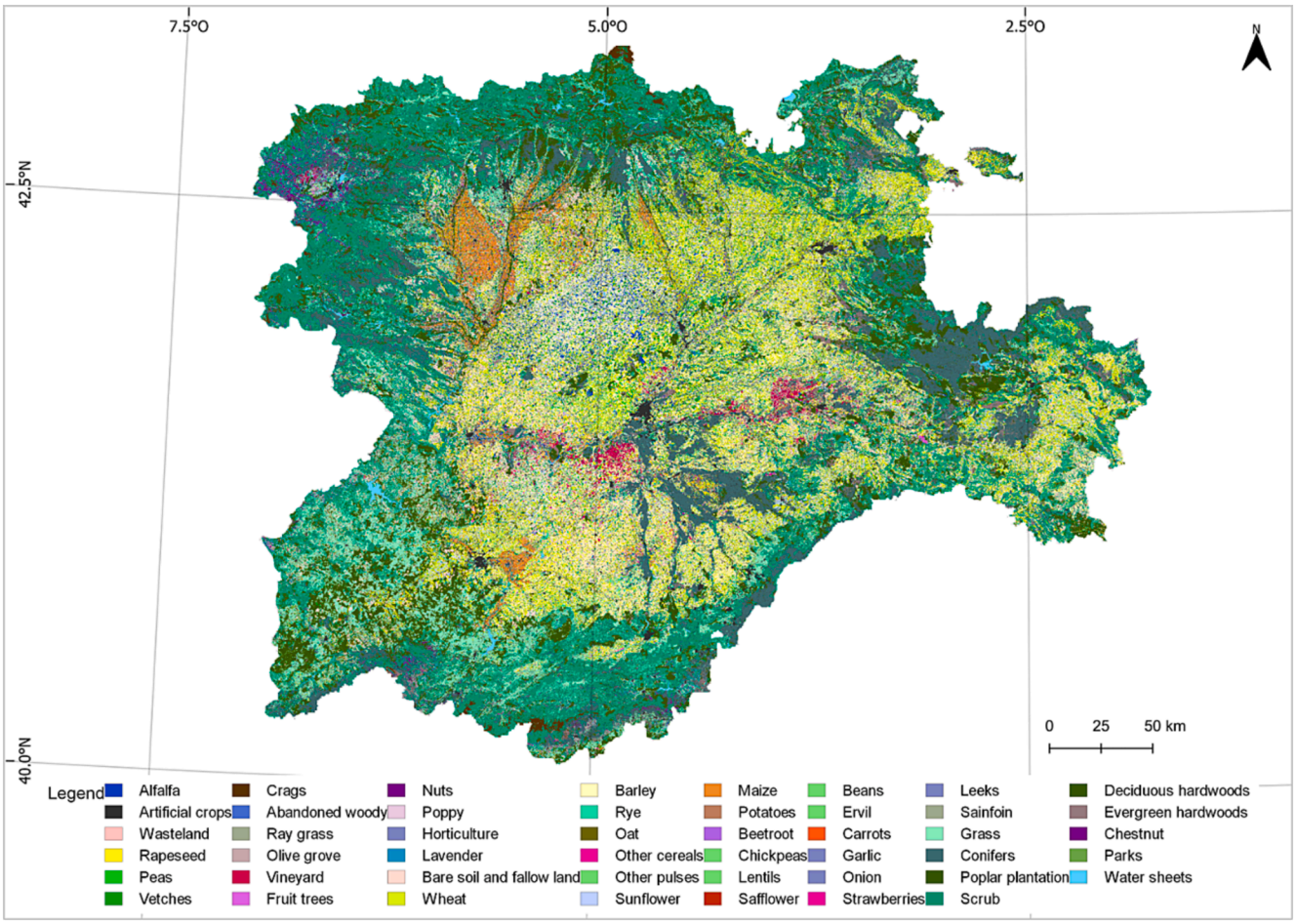

Fig. 2. Map of crops and natural areas of Castilla y León in 2021.

Table 1
Arable land with cereal crops in Castilla y León in 2021.

Crop	Area
Wheat	893,415 ha
Barley	855,541 ha
Maize	143,446 ha

inputs: the clearness index (K_t), – ratio of the global horizontal irradiance at ground level and the extra-terrestrial global solar irradiance on the horizontal plane –, the diffuse fraction (K_d) –the ratio of diffuse horizontal radiation to global horizontal radiation–, sky brightness (Δ), dew point temperature (T_d), and the cosine of the solar zenith angle. There are also other empirical models that require fewer inputs to obtain *PAR* estimates such as the one by Aguiar et al. (2012), which only requires the *GHI* and K_t to develop the model, or the one proposed by Foyo-Moreno et al. (2017) to estimate *PAR* under all sky conditions using θ_Z and K_t as input parameters. García-Rodríguez et al. (2021) included K_t, K_d, the direct fraction (K_b) –the ratio of direct beam to total radiation–, ε, Δ, cloud cover (*CC*), air temperature (*T*), pressure (*P*), the cosine of the solar azimuth, and *GHI* and then, employed two strategies for modelling *PAR*: multilinear regression, and Artificial Neural Networks (ANNs).

Another option is the use of satellite observations for a specific state of the atmosphere. Among others, Rubio et al. (2005) developed a model to estimate solar irradiance under cloudy conditions and then, combined it with a model to estimate *PAR* from *GHI*. Wang et al. (2020) used Level-3 (L3) MCD18A2 Moderate Resolution Imaging Spectroradiometer (MODIS)-derived *PAR* in the shortwave spectrum from NASA geostationary (Terra and Aqua) satellite data.

In general, the extinction coefficient is a parameter that describes the attenuation of light as it passes through different surfaces. In a crop canopy, the light extinction coefficient (k) refers to the efficiency of light interception. Both plant canopy characteristics (development stage (Sieling et al., 2016), leaf shapes, and inclination angles) and the spectral properties of solar radiation, such as the solar elevation angle (Kukal and Irmak, 2020) influence the calculation of the light extinction coefficient. Although studied as a coefficient over many years, it was only a few decades ago that its utility could really be seen in direct application to crop modelling. Despite being able to calculate it for a complete growing season (Kukal and Irmak, 2020), there are authors who have successfully achieved daily k values for maize (Drouet and Kiniry, 2008) and even hourly k values for barley (Tabarzad et al., 2016).

The third parameter that determines the Beer-Lambert Law is the Leaf Area Index (*LAI*). *LAI* is the leaf area per unit ground projection area (m^2/m^2) (Wei et al., 2020). It is a reliable indicator of the state and evolution of vegetation over time and all leaf types, both green and senescent (Anderegg et al., 2023). *LAI* can be estimated through both direct and indirect methods (Sebastiani et al., 2023). Direct methods are more accurate, as they require in situ sampling and data post-processing, as with harvested leaves and the leaf litter method. Indirect optical methods measure light transmission using the Beer-Lambert Law (Monsi and Saeki, 2005), gap fraction theory (Lang and Yueqin, 1986), and Digital Hemispherical Photography (DHP). In recent years, other methodologies have been developed, such as machine-learning processing of remote sensing data (Fang et al., 2019). Leaves have quite

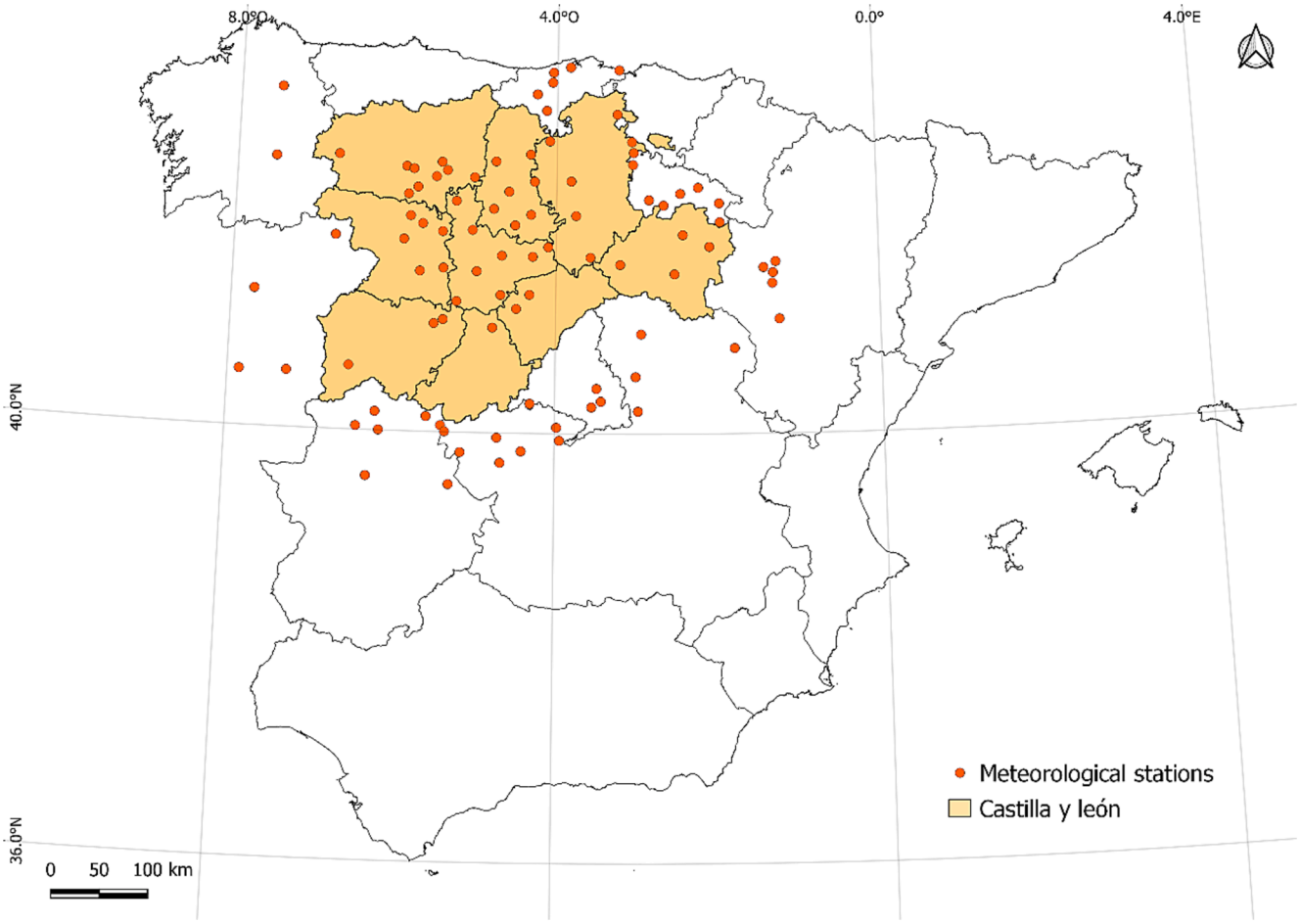

Fig. 3. Locations of the 93 meteorological stations.

Table 2
Technical specifications of pyranometers.

Network	Model	Spectral range	Calibration uncertainty
AEMET	CMP11 and CMP21, Kipp & Zonen	285 to 2800 nm	± 1 %
CIMA	095, Met One Instruments	285 to 2800 nm	± 3 %
IPMA	Kipp-Man CM11, Kipp & Zonen	310 to 2800 nm	± 3 %
SiAR	Skype SP1110, Campbell Scientific	350 to 1100 nm	± 3 %

Table 3
Light extinction coefficient (k) estimated values for each cereal crop.

Crop	*k*	Reference
Wheat	0.52	(Liu et al., 2021b)
Barley	0.44	(Ramirez-Garcia et al., 2012)
Maize	0.37	(Farré and Faci, 2006)

different optical characteristics, absorbing more radiation near the visible spectrum than in the infrared, so spectral measurements are strongly related to leaf density, and therefore to *LAI* (De Kauwe et al., 2011).

Some authors express *IPAR* over a complete growing season as a cumulative figure (*CIPAR*). They take days after sowing as a reference to make their *IPAR* measurements and add them all together at the end of the crop cycle (Tarkalson et al., 2012; Liu et al., 2021). Others calculate the fraction of Intercepted Photosynthetically Active Radiation (*fIPAR*) as a ratio of the intercepted *PAR* to the incident *PAR* (Wojnowski et al., 2021).

The main objective of the article is to define a basic methodology to determine the average annual growth and yield patterns for large crop areas using different data sources, by estimating the monthly *IPAR* values calculated from the Beer Lambert equation. The procedure has been studied in the case of maize, barley and wheat crops in the extensive region of Castilla y León, Spain. A globally calibrated *PAR* estimation model, using *GHI* data recorded in Burgos (Spain), *LAI* satellite data and *k* literature data. Spatial GIS representations of the variable are very helpful as they provide information on monthly *IPAR* within each plot. The research is completed with the calculation of the *fIPAR* in different provinces to determine the percentage of *PAR* actually used by cereals for photosynthesis out of all the incident *PAR* they receive. Furthermore, they are related to the average yield data of the three cereals in the provinces to establish whether there is a relationship with *fIPAR*. In this way, the importance of studying variables such as the solar radiation and its influence on the planning of agricultural campaigns is highlighted.

The work is structured as follows: after the Introduction Section, the methodology is presented in Section 2 with a description of the location and the climate of the study area, data acquisition and treatment procedures, the production of crop maps, and both the *PAR* and the *IPAR* estimations. Section 3 is divided into the following four subsections:*GHI*, *PAR*, *LAI*, and *IPAR*. In each one, relevant results are described and displayed in spatial representations. The following section is the discussion of the results. Finally, the conclusions are summarized in Section 5.

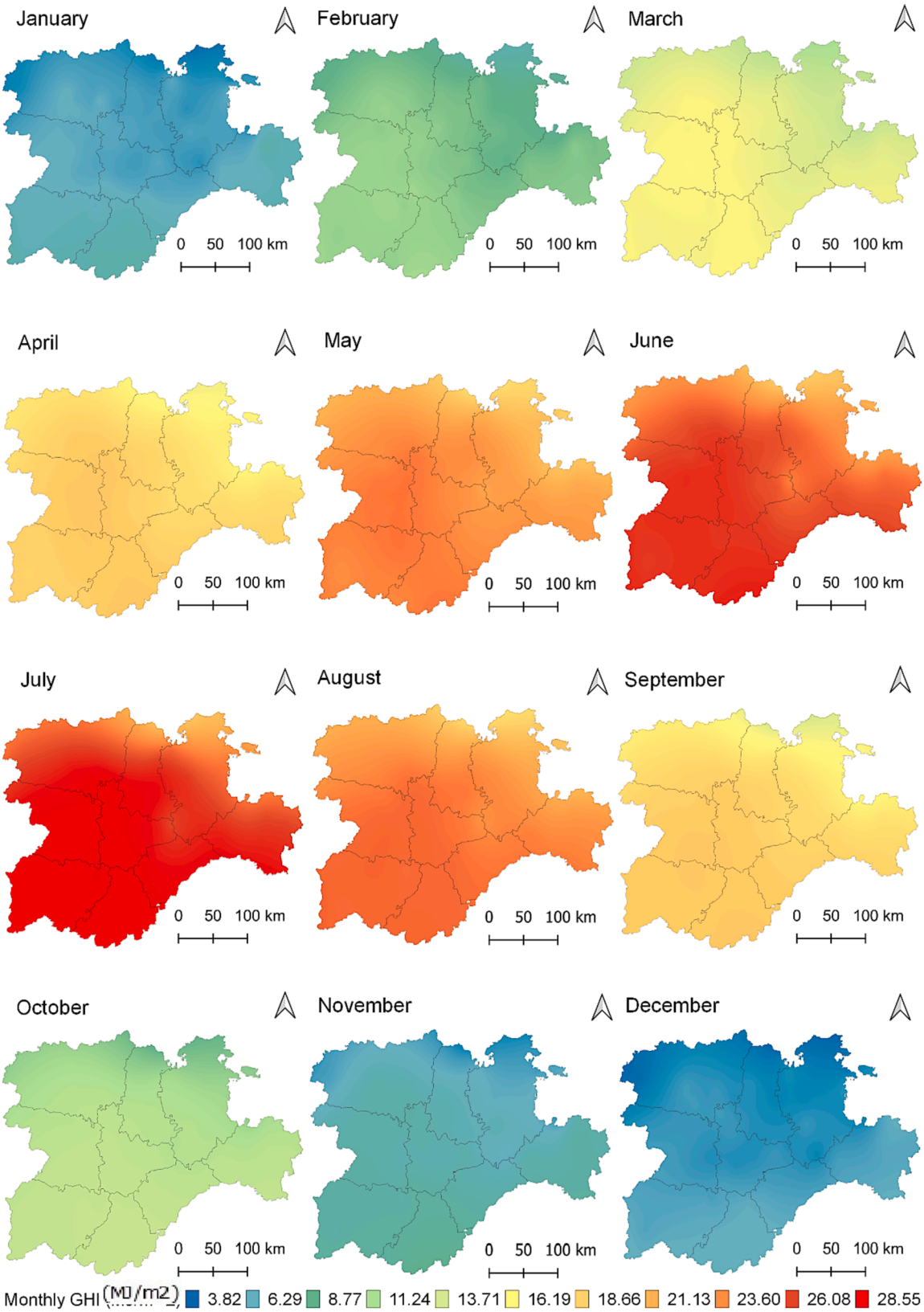

Fig. 4. Monthly mean of daily *GHI* maps in Castilla y León.

Table 4
Error rate of the UK interpolation method with four control treatments.

	Weather stations	nRMSE (%)	nMBE (%)	nMAE (%)
Control 1	BU05, SA101, SG02, VA101, ZA02, ZA08	10.12	−0.61	2.19
Control 2	LE03, LE06, ZA04, ZA05, ZA08, VA08	5.14	0.79	1.03
Control 3	LE02, VA01, VA08, PA07, PA04, BU04	4.27	0.13	0.37
Control 4	PA01, PA06, BU04, BU05, VA101, SO01	5.55	0.04	0.39

2. Methodology

2.1. Location and climate

One of the largest regions in Europe and the largest in the Iberian Peninsula, Castilla y León has a surface area of 94,224 km^2. Located inland in northwest Spain (Fig. 1), a broad meseta dominates the region with an average altitude of 800 m. Its distinctive orography has three mountain systems (the Cantabrian Mountains to the North, the Central System to the South, and the Iberian System to the East). As a result, its climate is mainly cold semi-arid on the central plateau or meseta, although other temperate and cold climate varieties also characterize the boundary areas of the region, according to the Köppen-Geiger climate classification (Beck et al., 2018).

BSk: Cold semi-arid steppe; Csa: Temperate with hot dry summer; Csb: Temperate with warm dry summer; Cfb: Temperate with no dry season and with warm summer; Cfc: Temperate without dry season and with cold summer; Dsb: Cold with warm dry summer; Dsc: Cold with cold dry summer; Dfb: Cold without dry season with warm summer; Dfc: Cold without dry season with cold summer.

2.2. Crop maps

The "Mapa de Superficies Naturales de Castilla y León 2021" (MSNCyL), an annual publication of the *Instituto Tecnológico Agrario de Castilla y León* (ITACyL) (Instituto Tecnológico Agrario de Castilla y León, 2022), was used to identify the different types of crops and the area of land that each one occupied (Fig. 2).

Despite the wide variety of crops grown in Castilla y León, the most representative cereals such as wheat, barley, and maize were cultivated in a total area of 1,892,402 ha in 2021 (Table 1), representing 90 % of the arable land used for cereals within Castilla y León (Ministerio de Agricultura, Pesca y Alimentación, 2021).

2.3. Global horizontal irradiance data acquirement and treatment

Experimental mean daily *GHI* data (MJ·m^{-2}) were collected at the 93 stations specified in Fig. 3, covering the wide variety of regional topographic and climatic characteristics. All the stations are detailed in Tables A1 and A2 of the appendix with their coordinates and corresponding climatic variations.

Mean daily *GHI* data (MJ·m^{-2}) were used from 46 weather stations in Castilla y León (Table A1) and 47 stations (Table A2) in neighbouring regions of Spain and Portugal, all recorded over a period of 14 years (2007–2020): respectively, *InfoRiego* - (Instituto Tecnológico Agrario de Castilla y León Junta de Castilla y León, 2022) for data in Castilla y León; and *Sistema de Información Agroclimática para el Regadío* (SiAR network) (Ministerio de Agricultura Pesca y Alimentación, 2022), *Agencia Estatal de Meteorología* (AEMET) (Ministerio para la Transición Ecológica y el Reto Demográfico, 2022); *Centro de Investigación del Medio Ambiente* (CIMA) (Consejería de Desarrollo Rural Ganadería Pesca Alimentación y Medio Ambiente Gobierno de Cantabria, 2022); and *Instituto Português do Mar e da Atmosfera* (IPMA) (Instituto Português do Mar e da Atmosfera, 2022), for data collected in neighbouring regions.

Among all the stations located in each Community, those with more than 12 years of available data (a valid year equates with over 330 daily values) were selected. The technical specifications of the network pyranometers were as follows (Table 2):

The daily average of *GHI* (MJ·m^{-2}) for each month was therefore calculated to obtain the final monthly average of the total volume of data for each of the meteorological stations. The monthly average of daily *GHI* (MJ·m^{-2}) values were used to prepare maps with QGIS 3.16 software. Spatial interpolation techniques can produce a grid based on single values (Palmer et al., 2017), although kriging interpolation techniques are the most reliable for climate variables, such as solar radiation (Wen et al., 2023). Among the kriging interpolation techniques, the most robust over large areas are Ordinary Kriging (OK) (Alsamamra et al., 2009; Palmer et al., 2017) and Universal Kriging (UK) (Ertekin and

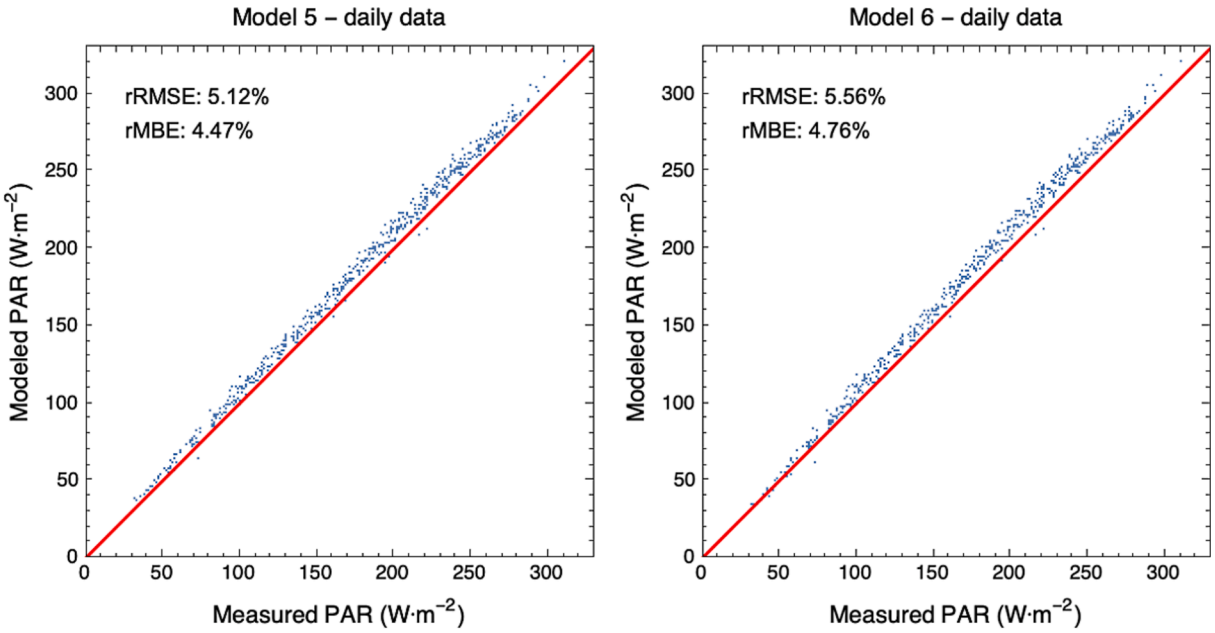

Fig. 5. Scattered plots for models 5 and 6 using daily *PAR* (W·m^{-2}) data from Burgos station.

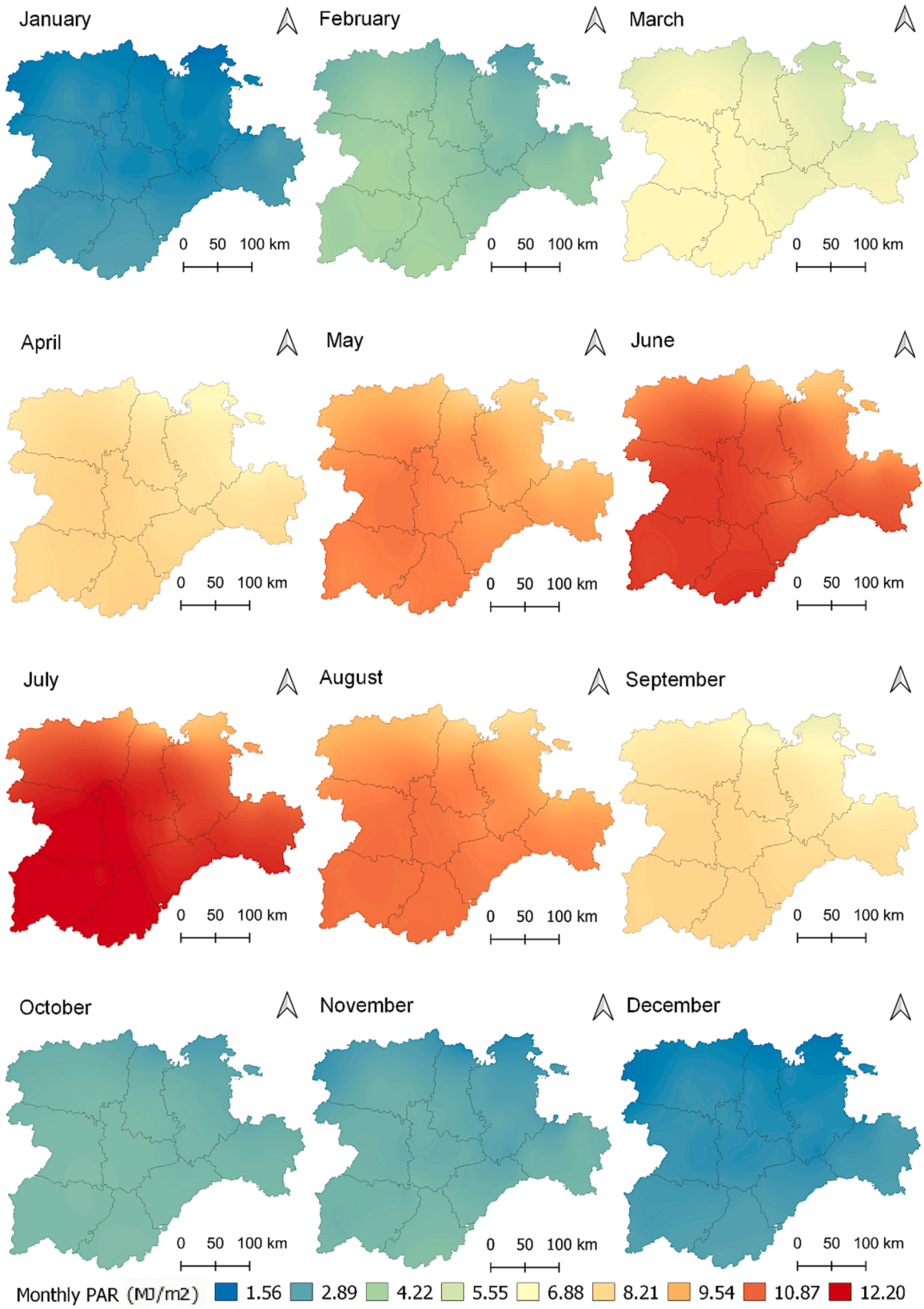

Fig. 6. Monthly mean daily *PAR* maps for Castilla y León.

Evrendilek, 2007; Rodríguez-Amigo et al., 2017), although factors such as the topographical complexity of the terrain may reduce its accuracy. Rodríguez-Amigo et al. (2017) yielded the lowest values for the statistical indicators normalized Root Mean Square Error (nRMSE) and normalized Mean Absolute Error (nMAE), 1.43 % and 1.26 % respectively, with the UK interpolation method with 35 stations and quadratic semi-variogram for Castilla y León. For this reason, the UK interpolation method was implemented in this study with the System for Automated

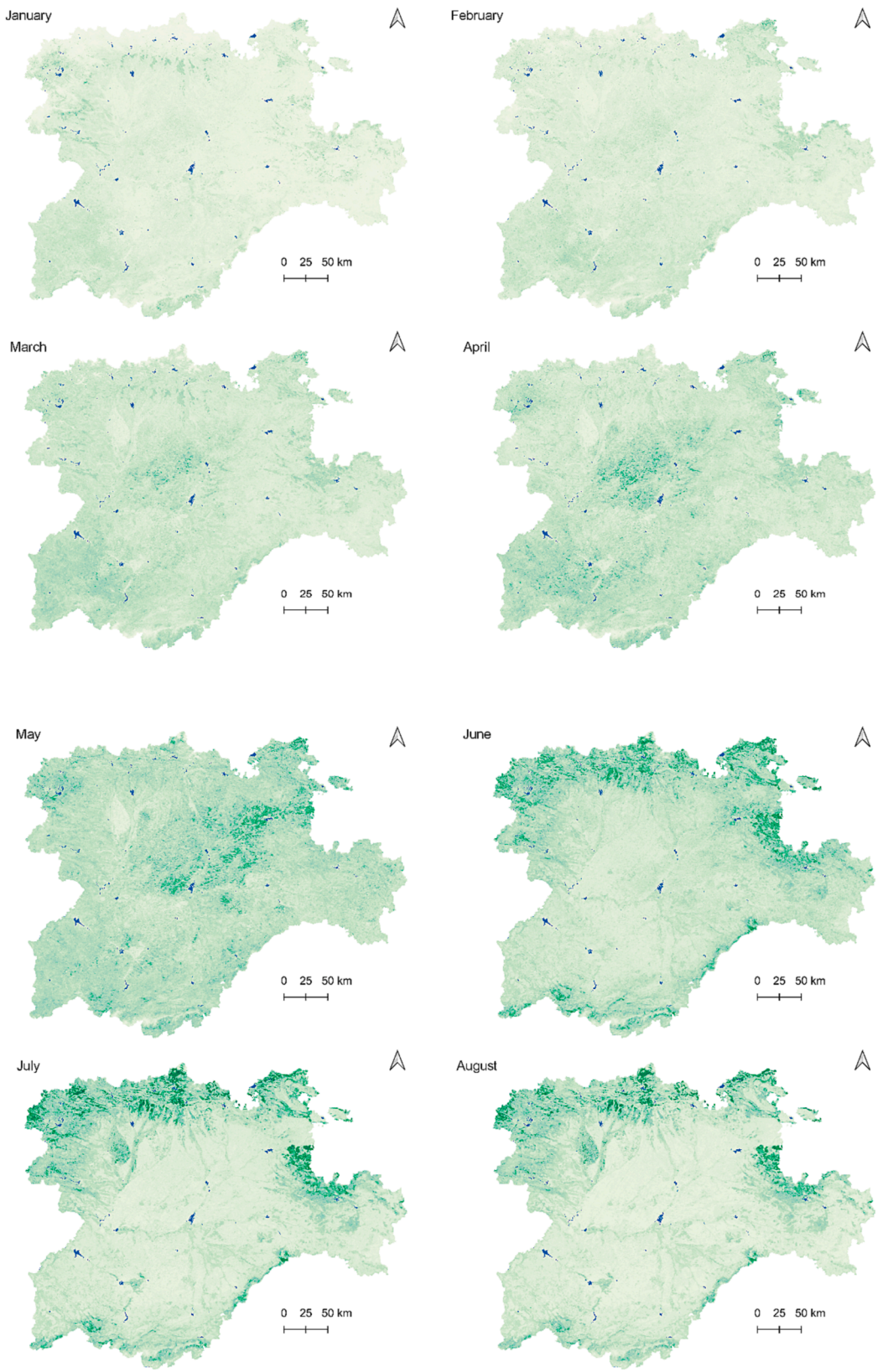

Fig. 7. Monthly maps of *LAI* within Castilla y León.

Geoscientific Analyses (SAGA) hybrid geographic information software, choosing the B-spline interpolation resampling and a global search range with all points within search distance.

2.4. Photosynthetically Active Radiation estimation

As previously mentioned, *PAR* databases are spatially and tempo-

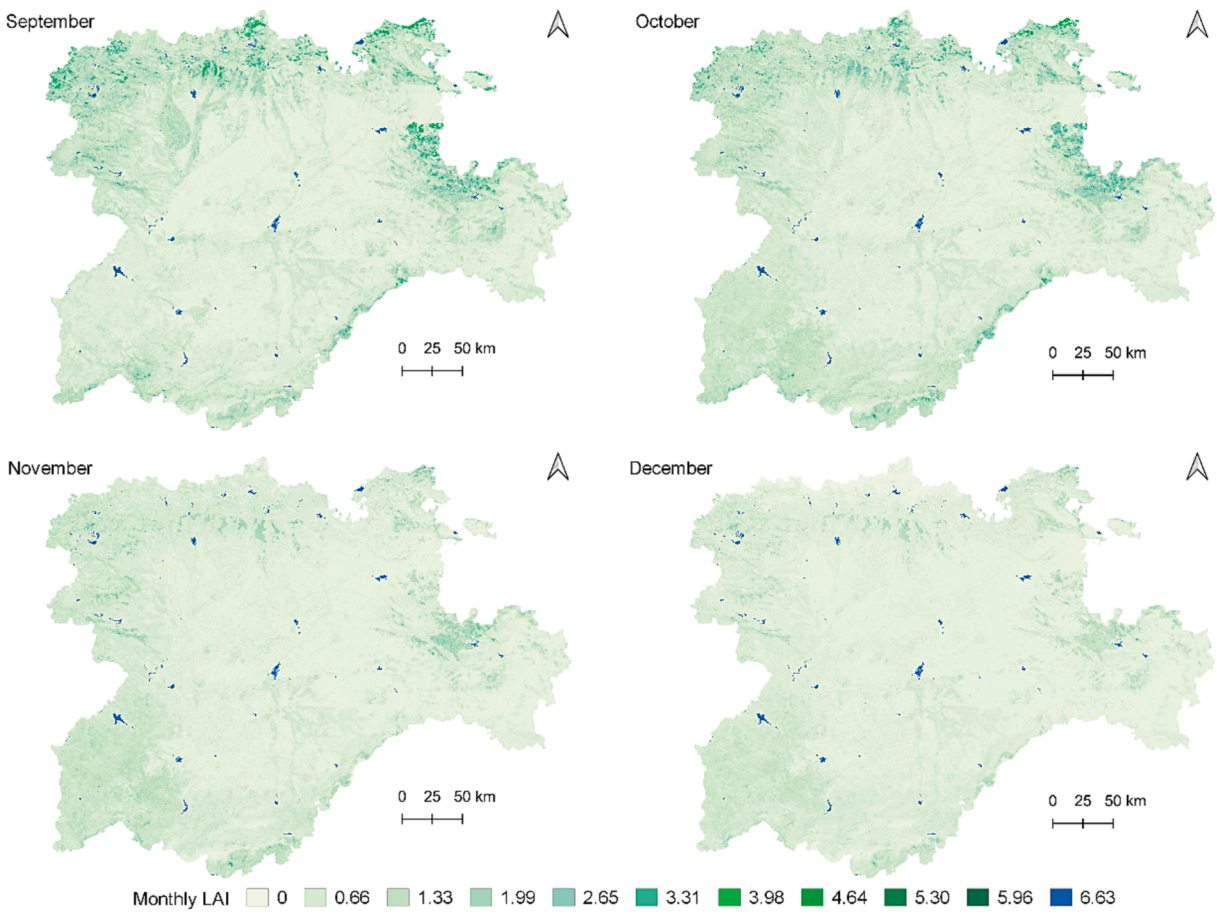

Fig. 7. (*continued*).

rally limited. In addition, taking field measurements is a very technical and time-consuming process, the precision of which is often difficult to ensure, and there is no official standard for the *PAR* measurement quality control (Mizoguchi et al., 2014). *PAR* was therefore calculated after applying two global calibrated models calculated in a previous work (de Blas et al., 2022). In this study, 21 models were calibrated with 1-min data from a 10-year long time series from the Surface Radiation Budget (SURFRAD) network, obtaining low fitting errors when 1-min fitted models were validated with daily data and for all sky conditions (clear, partial, and overcast). The models selected (named models 5 and 6 in (de Blas et al. 2022)) are the two most recent ones, whose inputs, *GHI* and K_t (Yu et al., 2015; Nyamsi et al., 2019), were expressed with the coefficients obtained after the global calibration (Eqn 1 and 2).

Model 5

$$PAR = GHI\,(0.415212 - 0.0350336\ln Kt) \tag{1}$$

Model 6

$$PAR = GHI(-0.0340535(lnKt)^2 - 0.0757318lnKt + 0.406944), \tag{2}$$

PAR and *GHI* are the monthly average of photosynthetically active radiation and daily monthly global horizontal irradiance, respectively, and K_t is the monthly average of the daily clearness index. To calculate the monthly averages of daily K_t, the values of extraterrestrial irradiance on the horizontal plane for each hour of the year were first calculated at each meteorological station. Subsequently, the aggregated daily values of this variable were obtained. The monthly averages of extraterrestrial irradiance were then calculated based on the total daily values. Finally, the monthly averages of daily K_t were obtained by dividing the measured *GHI* values by the calculated extraterrestrial irradiance values.

The two models were validated with mean daily *PAR* data measured at the meteorological facility located on the flat roof of the Higher Polytechnic School building (Universidad de Burgos) between February 2019 and August 2021. The details of this station are described by García-Rodríguez et al. (2020). Experimental *PAR* and *GHI* data were recorded every ten minutes (averages from 30 s). The reliability of these models was evaluated using the relative Root Mean Square Error (rRMSE) (Eqn 3) and relative Mean Bias Error (rMBE) (Eqn 4).

$$\mathrm{rRMSE} = \frac{1}{PAR_{\mathrm{exp}}}\sqrt{\frac{\sum_{i=1}^{n}\left(\mathrm{PAR_{mod}} - \mathrm{PAR_{exp}}\right)^2}{\mathrm{n}}}\cdot 100(\%) \tag{3}$$

$$\mathrm{rMBE} = \frac{1}{\overline{\mathrm{PAR}}_{\mathrm{exp}}}\frac{\sum_{i=1}^{n}\left(\mathrm{PAR_{mod}} - \mathrm{PAR_{exp}}\right)}{\mathrm{n}}\cdot 100(\%) \tag{4}$$

where n is the number of the experimental data used for fitting the models; PAR_{mod} are the modelled values of *PAR*; and PAR_{exp} is the experimental value of *PAR*.

2.5. Leaf area Index

LAI information was obtained from satellite imagery provided by the MODIS/Terra + Aqua Leaf Area Index/FPAR 4-Day L4 Global 500 m SIN Grid (MCD15A3H) (NASA) (Myneni et al., 2015). This product is a 4-day composite *LAI* dataset with 500-metre pixel resolutions, covering the period between 1st January and 31st December 2021. Once the images corresponding to the year 2021 were available, the monthly average of the images was calculated. In this way, a monthly *LAI* raster layer derived from 7 or 8 images was obtained for the region of Castilla y León.

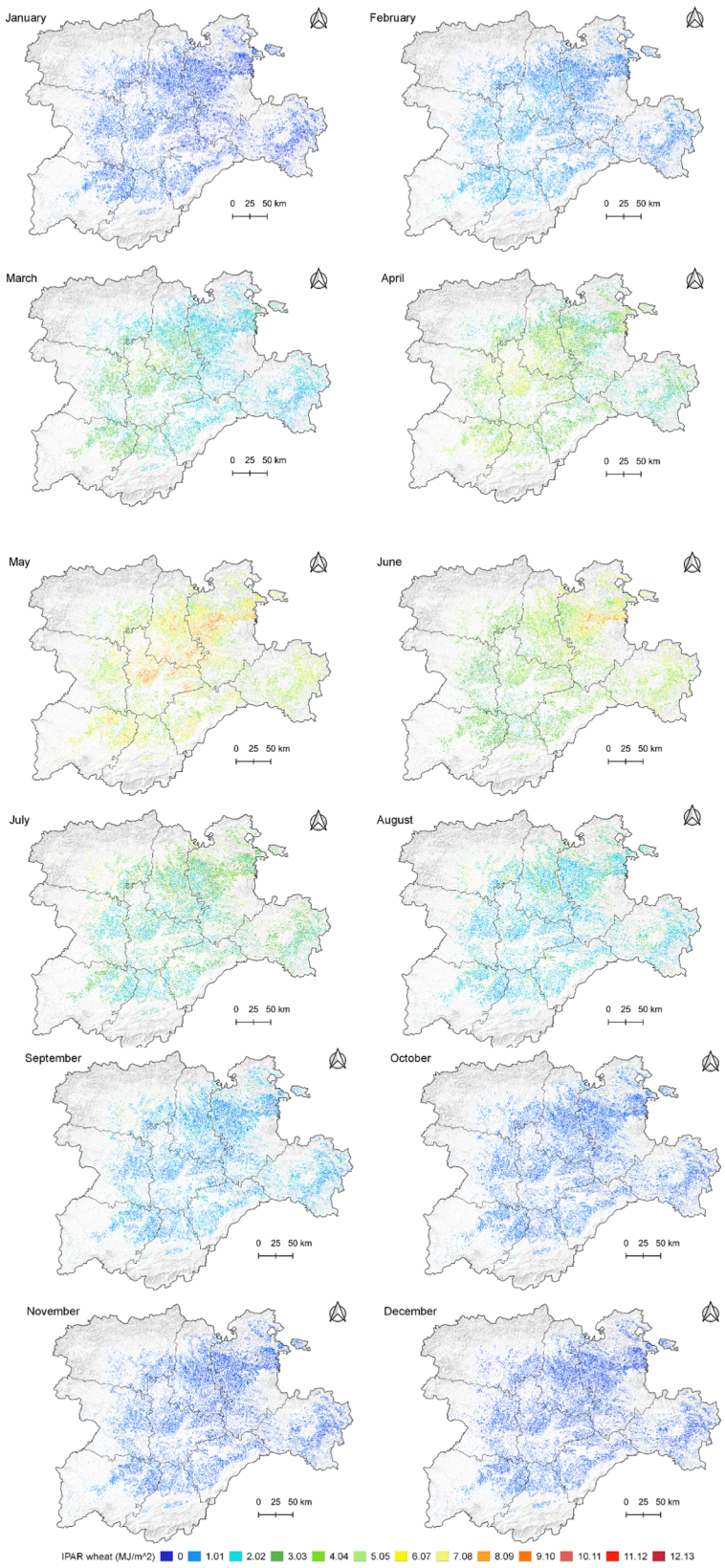

Fig. 8. Monthly *IPAR* maps for wheat crops within Castilla y León.

2.6. Light extinction coefficient

The *k* values (Table 3) were established after an extended literature review of different studies performed on these kinds of crops at several locations and under a wide range of environmental, physical, and chemical conditions. The criteria used for this selection were the closest locations to the region, and crop management as similar as possible to crop management in Castilla y León.

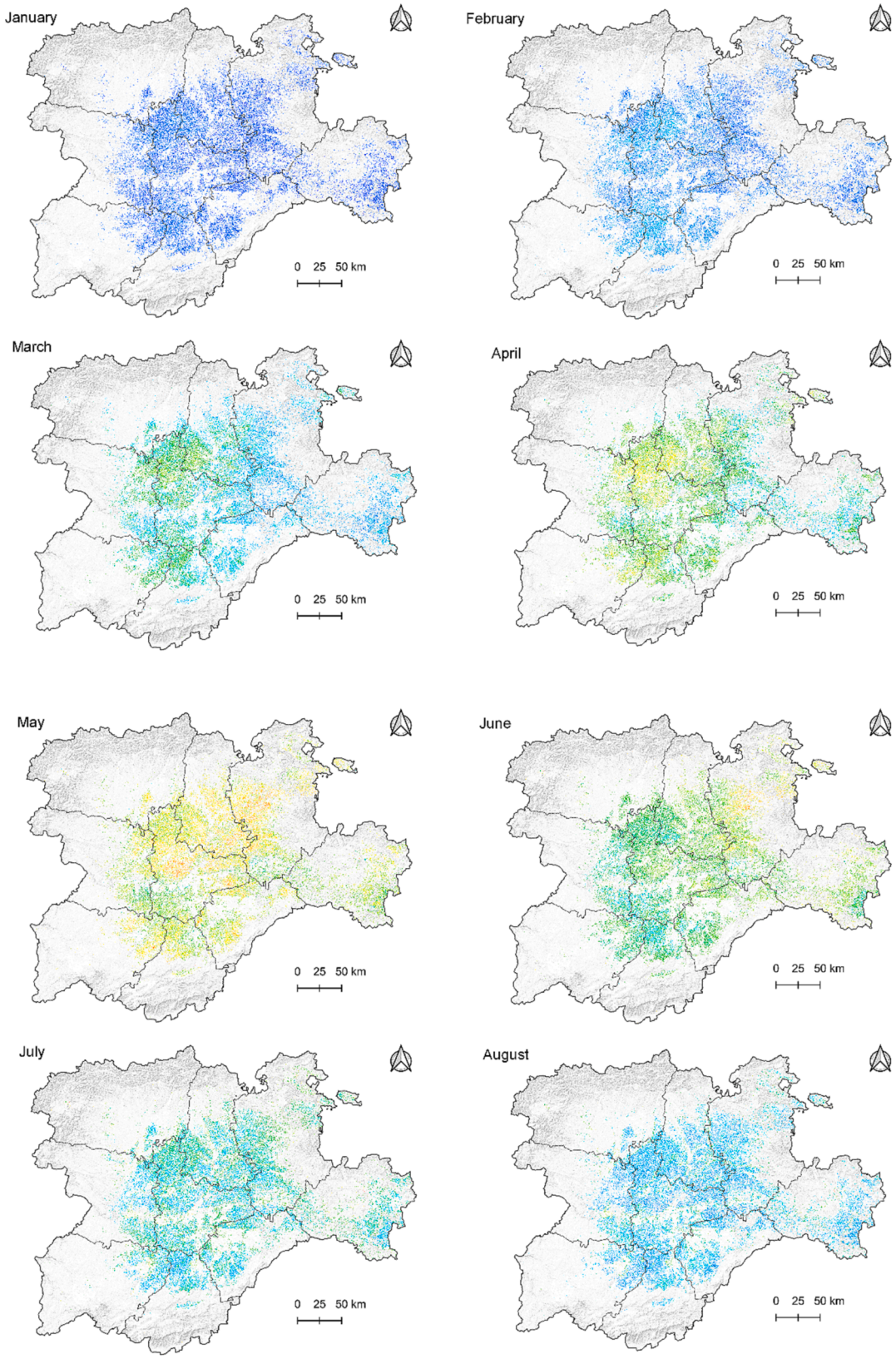

Fig. 9. Monthly *IPAR* maps for barley crops within Castilla y León.

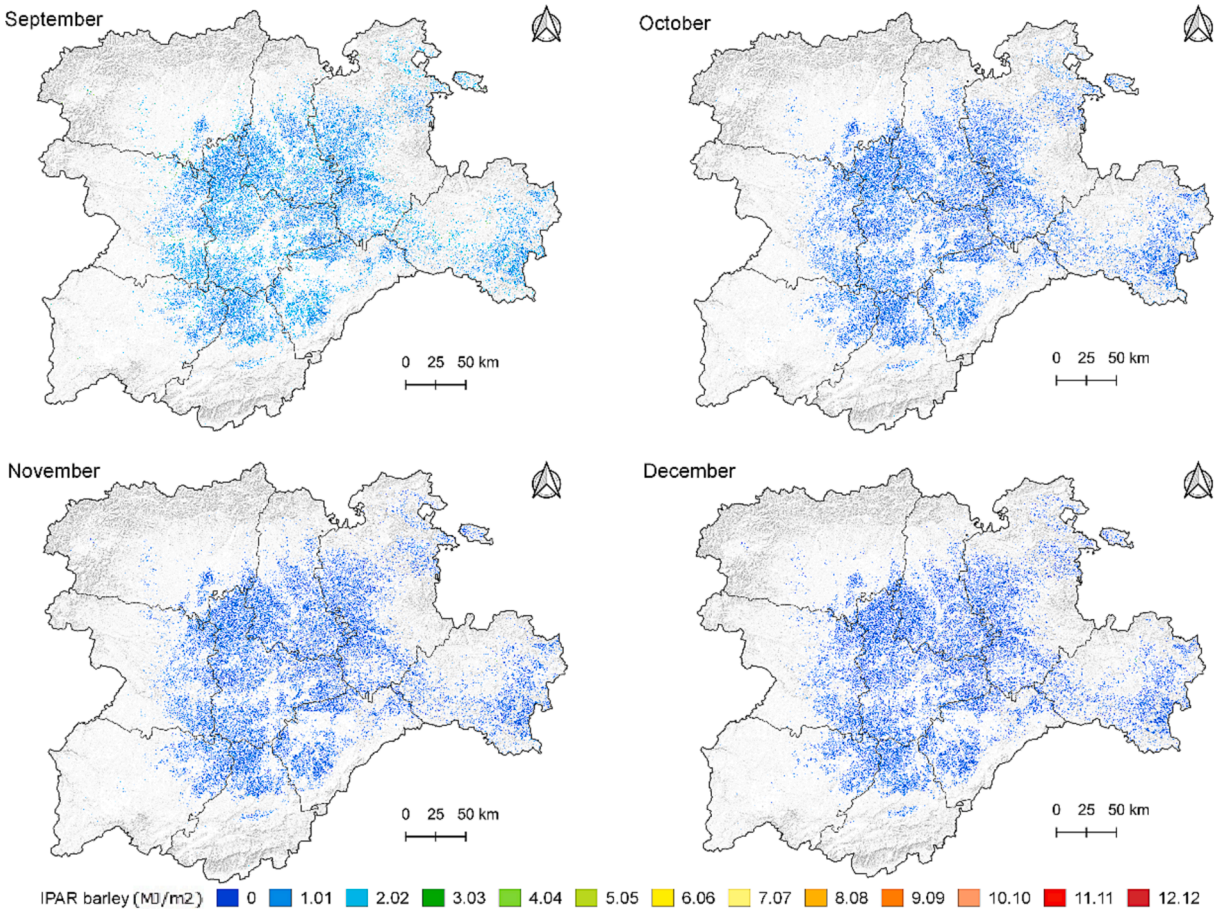

Fig. 9. (*continued*).

2.7. Intercepted Photosynthetically Active Radiation estimation

Finally, monthly *IPAR* maps for Castilla y León were obtained for each type of crop after applying the Beer-Lambert Law (Eqn 5). The pixel size of the *PAR* and *LAI* raster layers was unified to a size of 10 m by exporting these files with the desired resolution. After that, the Beer-Lambert Law could be applied to the whole extension of the Castilla y León region. To calculate this equation in each of the cereals, the *IPAR* raster layer for Castilla y León was applied to the wheat, barley, and maize raster layer. In this way, the *IPAR* values for each cereal were obtained.

$$IPAR = PAR \cdot \left(1 - e^{-k \cdot LAI}\right) \quad (5)$$

Once the monthly *IPAR* maps were obtained for each crop, the *fIPAR* for each cereal in all the provinces of the region was calculated (Eqn 6) (Wojnowski et al., 2021).

$$fIPAR = \frac{interceptedPAR}{incidentPAR} \quad (6)$$

3. Results

3.1. Spatial interpolation of global horizontal irradiance

Spatial representations (Fig. 4) were generated with the monthly means of daily *GHI* ($MJ \cdot m^{-2}$) values from the 93 stations (46 in Castilla y León and 47 in the neighboring Spanish and Portuguese regions). The ranges obtained for each month are shown in Table A3, and were, as expected, higher during the summer months, reaching the maximum value, 28.55 $MJ \cdot m^{-2}$, in July, in the westernmost area of the province of Salamanca. On the other hand, the minimum value recorded was 3.82 $MJ \cdot m^{-2}$, in the northern part of the province of Burgos in December.

In addition to these maps, a cross-validation of the mean daily *GHI* data was conducted with 4 permutations (Control 1 to 4) of 6 weather stations of Castilla y León (Table A1) and calculated the average values of nRMSE, nMBE and nMAE (Table 4). The weather stations were selected according to their location and the distance among them. In control 1, the weather stations are located in the central area of the region and they are slightly further apart. In control 2 they are located further West, in control 3 in the northernmost provinces and in control 4 in the East.

3.2. Validation of Photosynthetically Active Radiation estimation models using global horizontal irradiance data

The scattered plots of the two models (Eqn 1 and 2) used for estimating *PAR* data across Castilla y León (Fig. 5) showed a good fit when applying the global models to the measured data in Burgos, with a slightly higher rRMSE and rMBE in Model 6. Even so, these rRMSE values (5.11 and 5.55 %, respectively) were considerably lower than 10 %. Burgos has a Csb climate (temperate with warm dry summer), like many other areas of the region. For this reason, Model 5, the one with the lowest errors, was widely used throughout the region.

3.3. Estimation of Photosynthetically Active Radiation

Once the *GHI* layers were generated, Model 5 (Eq. (1) was applied to obtain monthly *PAR* layers.

The information was previously compiled in monthly raster layers (Fig. 6). The ranges obtained for each month are shown in Table A4. As

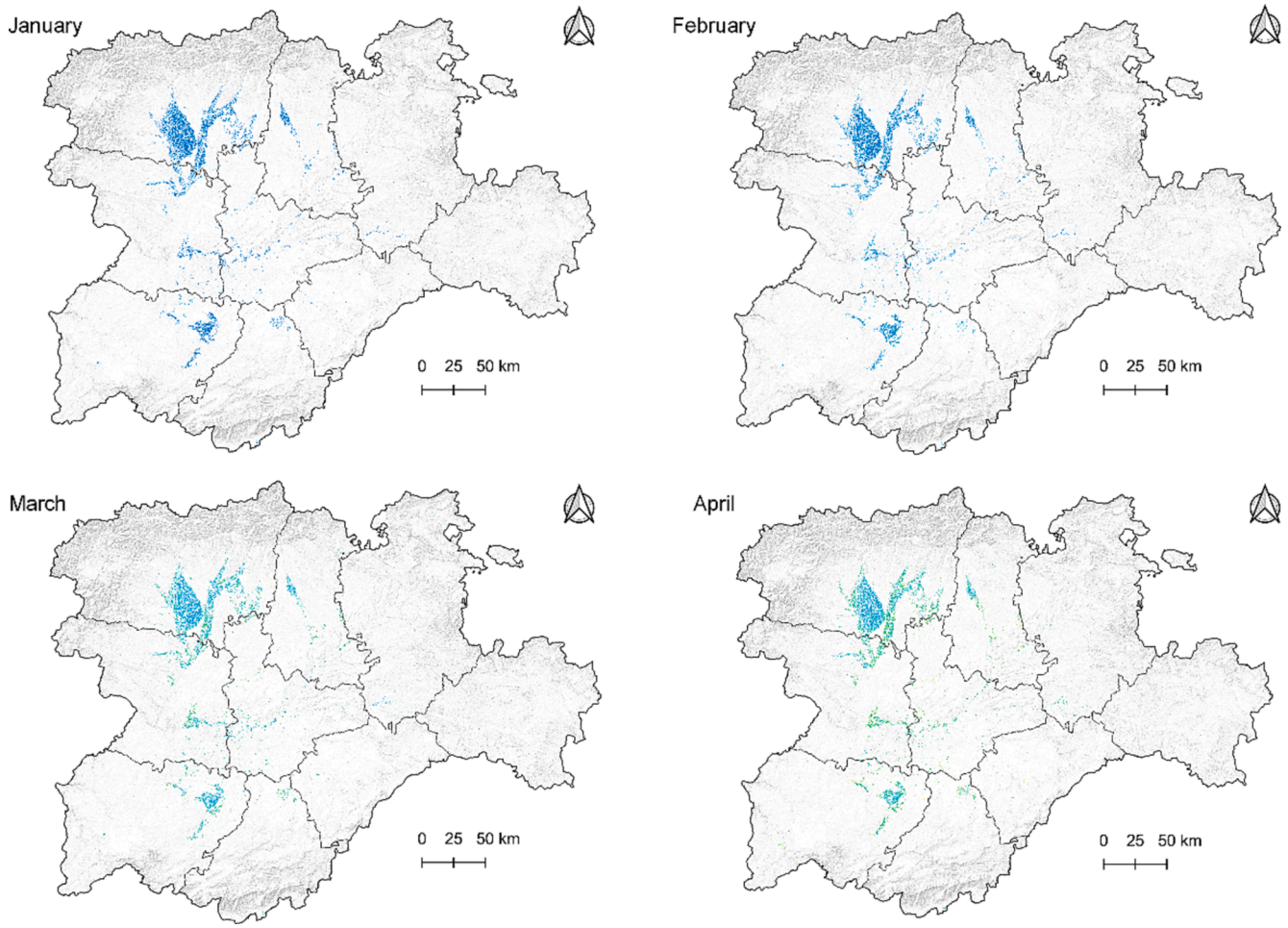

Fig. 10. Monthly *IPAR* maps for maize crops within Castilla y León.

is the case with *GHI* (MJ·m^{-2}) data, *PAR* (MJ·m^{-2}) values were highest during the months of May to August and the minimum values were for the months of December and January(Table A5).

3.4. Leaf area Index

Monthly *LAI* data was obtained from satellite imagery to work with them as raster layers (Fig. 7). In terms of leaf morphology, the leaves of the three cereals are lanceolate, the base is elliptical, and the apex is pointed, but in the case of maize they are much larger. As this is a monthly study, the evolution of the different cereals is seen throughout the year. In the winter and spring months their leaves are green and high values could be reached in the *LAI* on a few occasions, although generally, for cereal crops their ranges vary from 0 to 6.

3.5. Intercepted Photosynthetically Active Radiation

Once the *PAR* and *LAI* maps of Castilla y León were represented and a *k* value for each crop was chosen from the literature review, the Beer-Lambert Law could be applied to obtain the *IPAR* maps for wheat (Fig. 8), barley (Fig. 9), and maize (Fig. 10). The crop surfaces are represented on a color scale over a Digital Terrain Model (DTM) of all the provinces of Castilla y León. Table A6 shows the range of values obtained in each of the monthly *IPAR* maps.

These maps provide an estimation of *PAR* (MJ·m^{-2}) values that could be intercepted by wheat, barley, and maize. The values vary depending on the month of the year and the location within the Community so it was decided to study the fraction of Intercepted Photosynthetically Active Radiation (*fIPAR*) of each province. In Castilla y León, wheat and barley, whose morphology is very similar, ripen at the end of spring (Table 5).

For that reason, they are able to intercept more incident *PAR* in May and June. Fig. 11 shows how in February the percentages of *fIPAR* are lower than those recorded for wheat in June. In February, almost 50 % of the area of Burgos and León reaches percentages of *fIPAR* between 15 and 20 %. The provinces of Ávila and Salamanca, being located further south, have a higher percentage of area capable of reaching *fIPAR* vales between 25 and 45 %. In the month of June, more wheat area achieves higher percentages of *fIPAR*. The provinces of Burgos, Palencia and Soria, located in the north-east of the Community, have the largest wheat area (almost 50 %) able to intercept more than 45 % of the incident *PAR*.

In April the percentages of *fIPAR* reached by barley are higher than those of wheat in February (Fig. 12). Consequently, the crops are in a more advanced development stage and more area is able to intercept the incident *PAR*. Salamanca, Zamora, Valladolid and Palencia stand out for the barley area that intercepts more than 60 % of incident *PAR* in this month. In June, as in the case of wheat, the barley area in the provinces of Burgos, Palencia and Soria was particularly important, with a percentage of *fIPAR* over 40 %.

On the other hand, maize has a different vegetative cycle and it is not cultivated in all the provinces of Castilla y León. The provinces with the largest areas used for maize growing are León, Zamora and Salamanca. The maximum *fIPAR* percentages are reached in July (Fig. 13), the

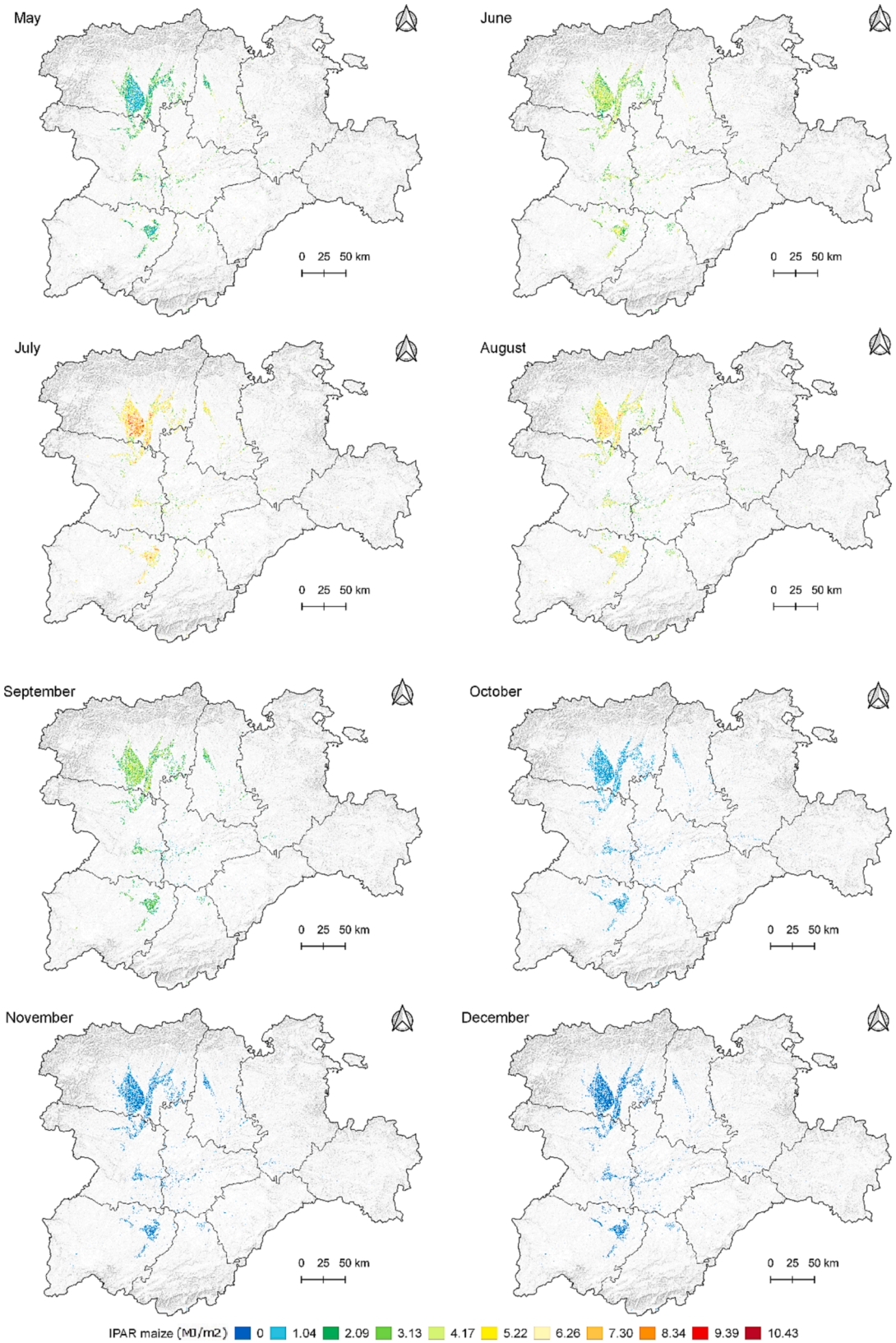

Fig. 10. (*continued*).

province of León have the highest percentage of area with a *fIPAR* over 50 %. In September, very little area exceeds these percentages of *fIPAR*, the most important being León with slightly more than 10 % of its maize area (Fig. 13).

The *IPAR* values recorded on the wheat and barley maps from July to December and the same for the months of November to April for maize are mostly due to the *PAR* levels, as crop plots are bare for harvesting. Afterwards, crop plots are left bare until sowing commences once again.

Table 5
Typical sowing and harvest months for cereals in Castilla y León.

Crop	Sowing month	Harvest month
Wheat	October - November	July - August
Barley	November - December	June - July
Maize	April - May	October - November

4. Discussion

The *GHI* values obtained for Castilla y León are similar to those obtained in the Autonomous Region of Andalucía (Alsamamra et al., 2009). Although higher monthly mean daily *GHI* values were recorded throughout the year, their *GHI* ranges were from 5 to 30 MJ·m-2 day, the minimum value being recorded in December and the maximum in July, as for the Autonomous Region of Castilla y León. Both regions have similar surface areas and a wide range of topographic and climatic characteristics. The statistical errors obtained for the UK interpolation in this study vary between 4.27 and 10.12 % for the nRMSE, the nMBE from −0.61 to 0.79 % and the nMAE between 0.37 and 2.19 %. These values are slightly higher than those reported by Rodríguez-Amigo et al. (2017) for the nRMSE, 1.43–5.10 %, but slightly lower for the nMBE, −0.08 to 3.19 % and for the nMAE, between 1.26 and 3.67 %. In their case, they also performed the UK interpolation with 4 different combinations, considering the number of stations (12 or 35) and the available variogram model (linear or quadratic).

A globally calibrated model was applied to calculate *PAR* values. The rRMSE value obtained from the model, 5.12 %, was slightly higher than those obtained in previous studies (de Blas et al., 2022; García-Rodríguez et al., 2022). This model offered very good results under different sky conditions, 3.5–7.5 % rRMSE and using data from SURFRAD local stations belonging to different climates (de Blas et al., 2022). Two of these stations, Boulder and Fort Peck, have the BSk (cold semi-arid steppe) climate, as do most of the stations located in Castilla y León. Their rRMSE values for the same model using daily data were 2.69 % and 3.49 %, respectively. The use of a global model is justified, as it provides very successful *PAR* results under different sky conditions and for different climates.

The satellite-derived *LAI* values depend on several factors such as the plant morphology or health (green or senescent), but the accuracy provided by satellite products is usually high. Despite the uncertainty they may introduce into the results, numerous studies use *LAI* satellite data as input to their performances, showing a coefficient of determination (R^2) of 0.55 and 0.52 for Landsat 8 and Sentinel-2 products, respectively, in a Mediterranean *peri*-urban forest (Sebastiani et al., 2023) as well as the one in a China cornfield that *LAI* data (Sentinel-2 and Landsat) showed good consistency with in situ measurements, nRMSE of 0.64 % and 0.72 %, respectively (Yu et al., 2020). In addition, other studies with cereals in different locations have given maximum values of 5.5 for wheat and 6.5 for maize in July in China (Tan et al., 2020). Meanwhile, in the months of February and March, *LAI* values in some plots of Iran ranged from 1.96 to 2.95 (Kamali et al., 2020).

The provinces of Burgos and Palencia obtained average grain yields of 5,358 and 4,736 kg/ha for wheat and 4,035 and 4,497 kg/ha for barley, respectively (Consejo Económico y Social de Castilla y León, 2021). These values are higher than the Community average, corresponding to the high *fIPAR* percentages reached by a large part of the wheat and barley area in these provinces in the month of June, before harvest begins.

Most of the maize cultivated in the Community is located in the provinces of León, Zamora and Salamanca, representing 85 % of the total. The average crop yield in the province of León is 14,398 kg/ha, higher than the Community average (Consejo Económico y Social de Castilla y León, 2021). Moreover, León is the province with the highest percentage of its area capable of intercepting more incident *PAR*.

The three northernmost provinces of Castilla y León (León, Palencia

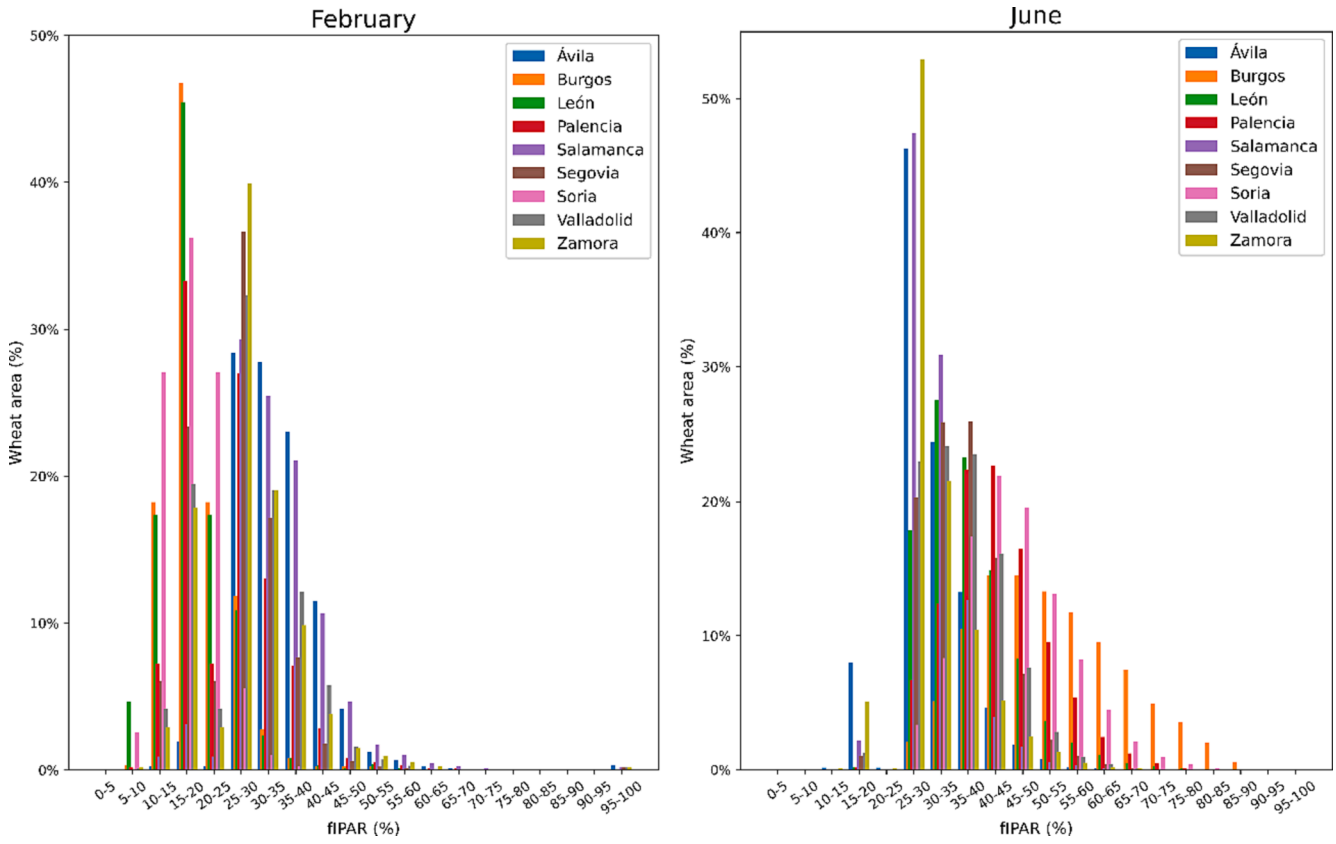

Fig. 11. Fraction of Intercepted Photosynthetically Active Radiation (*fIPAR*) (%) of wheat area (%) in February and June, in the all the provinces.

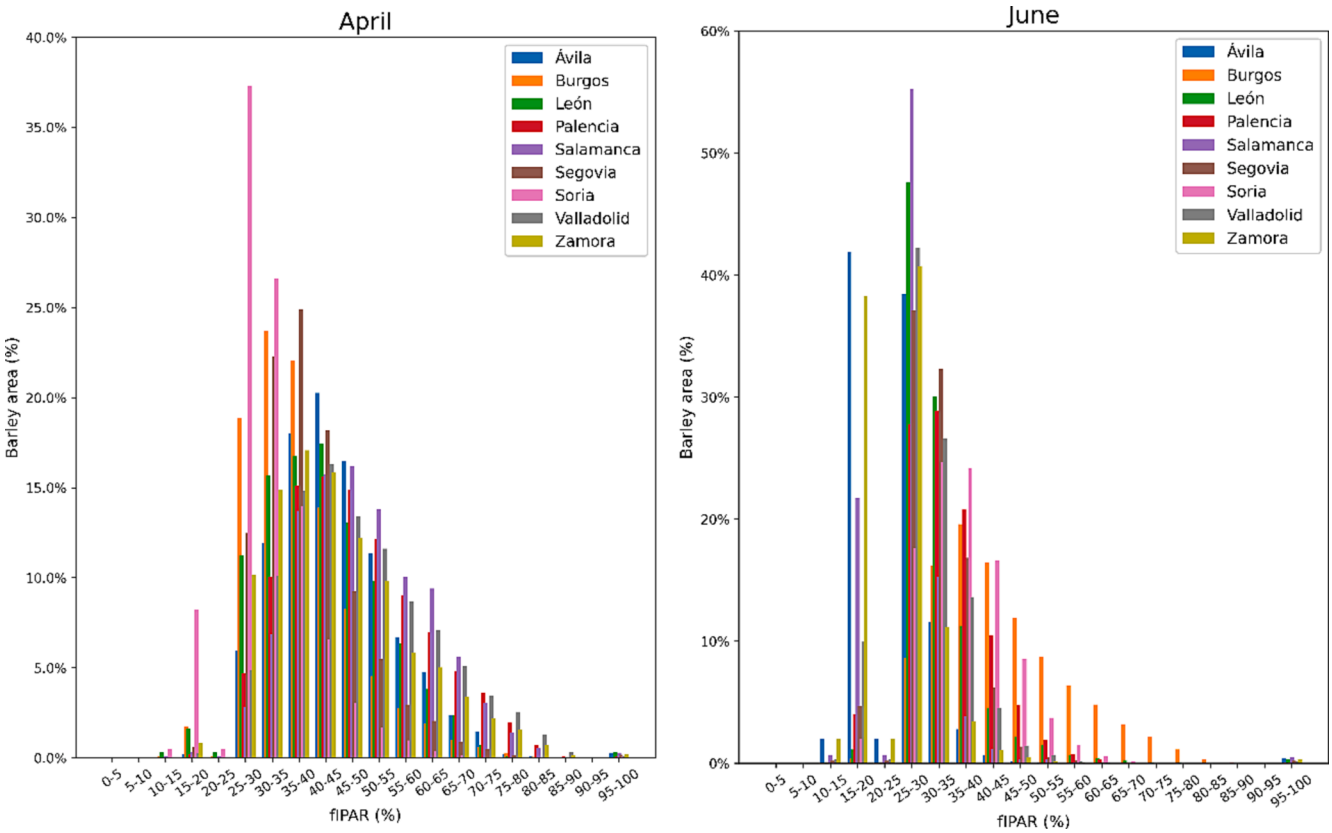

Fig. 12. Fraction of Intercepted Photosynthetically Active Radiation (*fIPAR*) (%) of barley area in April and June, in all the provinces.

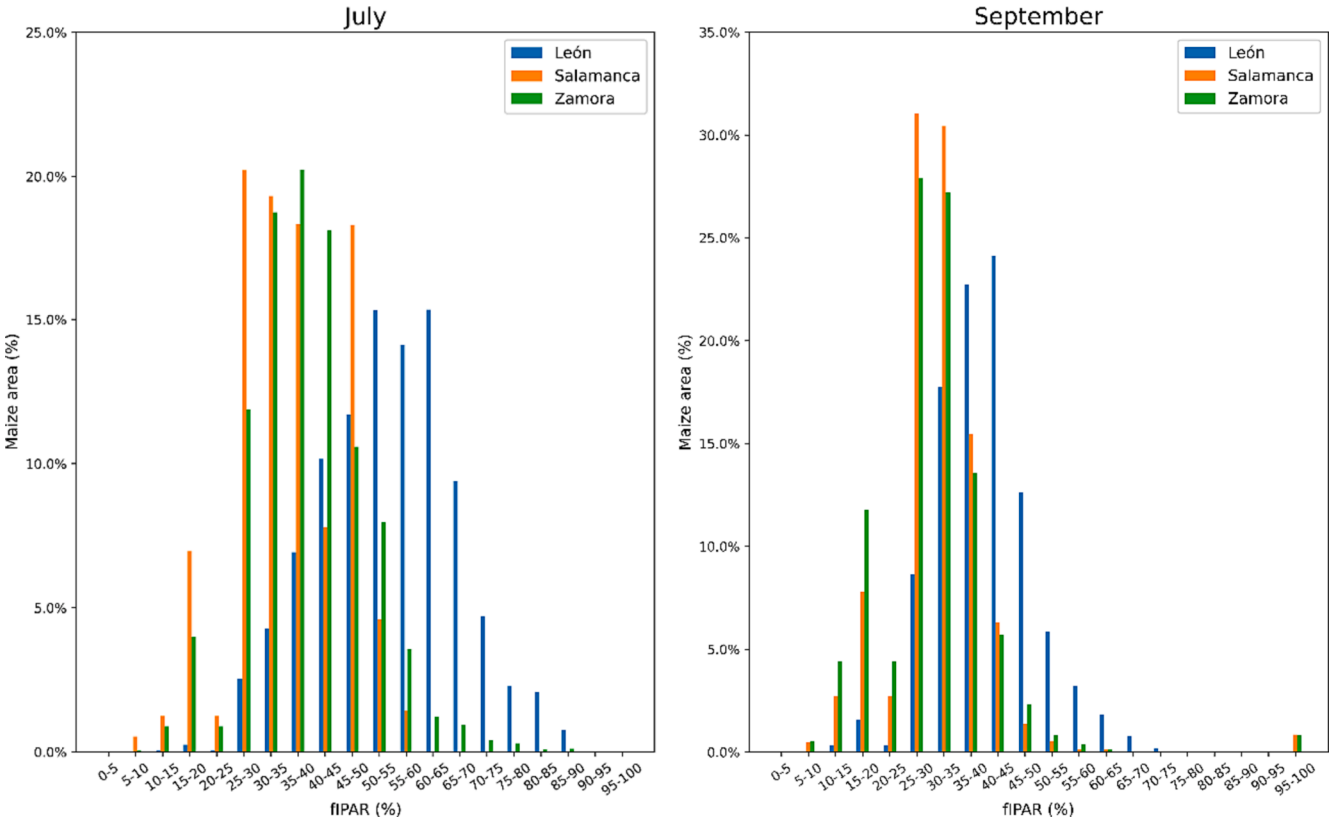

Fig. 13. Fraction of Intercepted Photosynthetically Active Radiation (*fIPAR*) (%) of maize area (%) in July and September, in León, Salamanca and Zamora.

Table A1
Meteorological stations within Castilla y León.

Name	ID station	Province	Latitude	Longitude	Köppen-Geiger climate classification
Nava de Arévalo	AV01	Ávila	40.978	−4.776	BSk
Valle de Losa	BU101	Burgos	42.718	−4.092	Cfb
Valle de Valdelucio	BU02	Burgos	42.026	−3.756	Cfb
Lerma	BU03	Burgos	42.347	−3.819	BSk
Tardajos	BU04	Burgos	41.639	−3.574	Cfb
Vadocondes	BU05	Burgos	42.715	−3.059	BSk
Santa Gadea del Cid	BU07	Burgos	42.971	−3.243	Cfb
Carracedelo	LE01	León	42.555	−6.734	Csb
Mansilla Mayor	LE02	León	42.509	−5.442	Cfb
Cubillas de los Oteros	LE03	León	42.373	−5.508	BSk
Zotes del Páramo	LE04	León	42.272	−5.736	BSk
Quintana del Marco	LE05	León	42.206	−5.851	BSk
Hospital de Órbigo	LE06	León	42.461	−5.884	Csb
Bustillo del Páramo	LE07	León	42.441	−5.792	Csb
Sahagún	LE08	León	42.372	−5.030	Cfb
Santas Martas	LE09	León	42.433	−5.372	Cfb
Torquemada	PA01	Palencia	42.033	−4.317	BSk
Villamuriel de Cerrato	PA02	Palencia	41.933	−4.515	BSk
Fuentes de Nava	PA03	Palencia	42.083	−4.783	BSk
Villoldo	PA04	Palencia	42.245	−4.596	BSk
Herrera de Pisuerga	PA06	Palencia	42.593	−4.332	Cfb
Villaluenga de la Vega	PA07	Palencia	42.524	−4.765	Cfb
Lantadilla	PA08	Palencia	42.341	−4.277	BSk
Ciudad Rodrigo	SA01	Salamanca	40.597	−6.523	Csa
Arabayona	SA101	Salamanca	41.008	−5.498	BSk
Aldearrubia	SA03	Salamanca	41.047	−5.386	BSk
Gomezserracín	SG01	Segovia	41.289	−4.326	BSk
Nava de la Asunción	SG02	Segovia	41.156	−4.487	BSk
Almazán	SO01	Soria	41.486	−2.533	BSk
Hinojosa del Campo	SO101	Soria	41.573	−3.205	Cfb
San Esteban de Gormaz	SO02	Soria	41.850	−2.428	BSk
Fuentecantos	SO03	Soria	41.739	−2.099	Cfb
Mayorga	VA01	Valladolid	42.150	−5.250	BSk
Finca Zamadueñas	VA101	Valladolid	41.218	−5.224	BSk
Torrecilla de la Orden	VA02	Valladolid	41.283	−4.683	BSk
Olmedo	VA03	Valladolid	41.733	−4.100	BSk
Encinas de Esgueva	VA05	Valladolid	41.500	−4.983	BSk
Tordesillas	VA06	Valladolid	41.643	−4.291	BSk
Valbuena de Duero	VA07	Valladolid	41.883	−5.043	BSk
Medina de Rioseco	VA08	Valladolid	41.649	−4.674	BSk
Colinas de Trasmonte	ZA01	Zamora	42.004	−5.817	BSk
Villaralbo	ZA02	Zamora	41.492	−5.685	BSk
Villalpando	ZA04	Zamora	41.865	−5.413	BSk
Pozuelo de Tábara	ZA05	Zamora	41.785	−5.892	BSk
Barcial del Barco	ZA06	Zamora	41.934	−5.664	BSk
Toro	ZA08	Zamora	41.526	−5.395	BSk

*BSk. Cold semi-arid steppe; Cfb. Temperate without dry season and with warm summer; Csb. Temperate with warm dry summer; Csa. Temperate with hot dry summer.

and Burgos) are the ones with the highest percentage of incident *PAR* intercepted. This could be due to the fact that part of their surface has Cfb and Csb climates, which may slow down the grain drying process.

The *IPAR* values increase during the late spring and early summer months are due to both the rising *PAR* and the advanced stage of development of wheat and barley. The same is true for maize in the summer and early autumn months (Hatfield, 2014). Therefore, it seems that, under right climatic and environmental conditions, crop yields are closely related to the amount of radiation intercepted during their growing season. Despite this, other factors such as optimal planting time, irrigation, intercropping time, sowing density, etc., also influence the final crop yield (Dzvene et al., 2023).

5. Conclusions

Globally estimated *PAR* models with robust *GHI* and *Kt* datasets, in combination with the *LAI* satellite data and *k* literature data have delivered satisfactory results for monthly *IPAR* levels in the three most common cereals of Castilla y León, wheat, barley and maize. This methodology can be used to analyze the average annual growth and the evolution of yield patterns in large crop areas under favorable conditions, even if some accuracy is lost. Certain variables and satellite imagery are particularly useful for estimating other variables quite reliably for which there is a scarcity of historical data series. The nRMSE values obtained from the *GHI* data interpolation are between 4 and 10 % approximately. The same is true for the error in the globally calibrated model, as both the rRMSE (5.12 %) and the rMBE (4.47 %) values are relatively low for these indicators. Although Beer Lambert's law applied in the current study yielded reasonable accuracies, further experiments to represent other essential variables could have improved the results. It would be interesting to validate the data obtained with experimental field measurements of both the *PAR* and *LAI* variables. Growth stage, sowing density or irrigation could be other factors to be considered to improve the precision of *IPAR* calculation. Wheat and barley reach their *IPAR* peaks in June and July with values between 11.56 and 12.13 $MJ{\cdot}m^{-2}$, while maize peaks in July and August with maximum values of 10.43 and 9.05 $MJ{\cdot}m^{-2}$, respectively. The location and, consequently, the climate, are also key factors in determining *fIPAR*. In the last months of development, the northernmost provinces of the community have a higher percentage of crop area which intercept more incident *PAR*.

Table A2
Meteorological stations within neighboring Spanish regions and Portugal.

Name	ID station	Province	Latitude	Longitude	Köppen-Geiger climate classification
Castro de Rei	LU01	Lugo	43.156	−7.486	Csb
Monforte de Lemos	LU02	Lugo	42.514	−7.523	Csb
Castro Urdiales	CAN01	Cantabria	43.383	−3.222	Cfb
CIMA	CAN02	Cantabria	43.357	−4.054	Cfb
Corrales de Buelna	CAN03	Cantabria	43.265	−4.063	Cfb
Guarnizo	CAN04	Cantabria	43.407	−3.838	Cfb
Los Tojos	CAN05	Cantabria	43.154	−4.257	Cfb
Reinosa	CAN06	Cantabria	43.002	−4.136	Cfb
San Román	LR02	La Rioja	42.234	−2.457	Cfb
Urbaña	LR03	La Rioja	42.175	−2.847	Cfb
Villoslada	LR04	La Rioja	42.125	−2.666	Cfb
Aguilar	LR05	La Rioja	41.967	−1.967	Bsk
Yerga	LR06	La Rioja	42.143	−1.972	Cfb
Foncea	LR07	La Rioja	43.156	−3.038	Cfb
Leiva	LR08	La Rioja	42.503	−3.046	Cfb
Ocón	LR09	La Rioja	42.289	−2.233	Cfb
Almonacid de la Sierra	Z01	Zaragoza	41.398	−1.324	BSk
Épila	Z05	Zaragoza	41.599	−1.280	BSk
Borja	Z14	Zaragoza	41.496	−1.315	BSk
Tarazona	Z15	Zaragoza	41.545	−1.432	BSk
Daroca	Z18	Zaragoza	41.065	−1.244	BSk
Center Finca Experimental	M01	Madrid	40.420	−3.492	BSk
Villa del Prado	M102	Madrid	40.276	−4.305	BSk
Arganda	M02	Madrid	40.301	−3.438	BSk
San Martín de la Vega	M05	Madrid	40.247	−3.553	BSk
Jadraque	GU02	Guadalajara	40.927	−2.947	BSk
Armuña de Tajuña	GU03	Guadalajara	40.530	−3.014	BSk
Prados Redondos	GU05	Guadalajara	40.796	−1.799	Cfb
Illana	GU06	Guadalajara	40.209	−2.986	BSk
Vegas de San Antonio	TO01	Toledo	39.956	−4.700	BSk
Los Navalmorales	TO04	Toledo	39.723	−4.657	BSk
Alcolea de Tajo	TO05	Toledo	39.814	−5.141	BSk
Recas	TO07	Toledo	40.056	−3.978	BSk
La Rinconada	TO09	Toledo	39.832	−4.404	BSk
Magán	TO11	Toledo	39.935	−3.942	BSk
Hurdes-Azabal	CC101	Cáceres	40.175	−6.184	Csa
Aldehuela del Jerte	CC04	Cáceres	40.003	−6.135	Csa
Peraleda de la Mata	CC09	Cáceres	39.514	−5.275	Csa
Jarandilla de la Vera	CC11	Cáceres	40.061	−5.385	BSk
Gargantilla	CC12	Cáceres	40.142	−5.563	Csa
Talayuela	CC13	Cáceres	40.004	−5.335	BSk
Coria-Puebla de Argeme	CC14	Cáceres	39.575	−6.272	BSk
Moraleja	CC16	Cáceres	40.036	−6.412	Csa
Vila Real	PORT02	Portugal	41.274	−7.717	Csb
Bragança	PORT03	Portugal	41.804	−6.743	Csb
Guarda	PORT04	Portugal	40.529	−7.279	Csb
Nelas	PORT05	Portugal	40.523	−7.855	Csa

*BSk. Cold semi-arid steppe; Cfb. Temperate without dry season and with warm summer; Csb. Temperate with warm dry summer; Csa. Temperate with hot dry summer.

Table A3
Ranges of *GHI* values estimated for Castilla y León.

Month	*GHI*(MJ· m^{-2})
January	4.15—7.59
February	7.09—11.09
March	11.09—15.73
April	14.90—19.59
May	17.74—24.50
June	18.89—27.23
July	19.33—28.55
August	17.37—25.09
September	13.77—19.45
October	8.91—13.31
November	4.82—8.48
December	3.82—6.62

Table A4
Ranges of *PAR* values estimated for Castilla y León.

Month	*PAR*(MJ· m^{-2})
January	1.56—2.96
February	2.71—4.36
March	4.94—6.85
April	6.62—8.53
May	7.87—10.59
June	8.38—11.72
July	8.55—12.20
August	7.66—10.74
September	6.08—8.37
October	2.68—3.60
November	2.15—3.73
December	1.72—2.92

Funding

This research forms part of project TED2021-131563B-I00, funded by MCIN/AEI/ 10.13039/501100011033 and by the "European Union NextGenerationEU/PRTR". Elena Garrachón-Gómez expresses her thanks to the Universidad de Burgos for the funding of her pre-doctoral contract. Ignacio García is likewise grateful to the Spanish Ministry of Universities and the European Union-Next Generation EU for their

Table A5
Ranges of mean monthly *LAI* values estimated for Castilla y León.

Month	*LAI*
January	0 – 4.06
February	0—4.23
March	0—4.63
April	0—5.51
May	0—6.40
June	0—6.54
July	0—6.59
August	0—6.63
September	0—6.32
October	0—5.73
November	0—4.38
December	0—4.4

Table A6
Ranges of *IPAR* values estimated for each crop in Castilla y León.

Month	*IPAR* wheat (MJ·m^{-2})	*IPAR* barley (MJ·m^{-2})	*IPAR* maize (MJ·m^{-2})
January	0—2.75	0—2.76	0.01—1.35
February	0—4.27	0—4.27	0.11—2.06
March	0—6.80	0—6.80	0.42—4.31
April	0—8.45	0—8.45	0.43—6.26
May	0—10.55	0—10.55	0.73—7.21
June	0—11.56	0—11.56	1.08—8.56
July	0—12.13	0—12.12	0.93—10.43
August	0—10.71	0—10.71	0.82—9.05
September	0—8.33	0—8.33	0.45—5.84
October	0—3.58	0—3.58	0.21—1.99
November	0—3.36	0—3.54	0.10—2.21
December	0—2.69	0—2.84	0.08—1.40

financial support (Program for the requalification of the Spanish university system 2021-2023, Resolution 1402/2021).

Declaration of competing interest

The authors declare that they have no known competing financial interests or personal relationships that could have appeared to influence the work reported in this paper.

Data availability

Data will be made available on request.

Acknowledgements

The authors wish to thank the Instituto Português do Mar e da Atmosfera for providing the mean daily global horizontal irradiance data from the four weather stations located in Portugal.

Appendix A

See Tables A1-A6

References

Aguiar, L.J.G., Fischer, G.R., Ladle, R.J., Malhado, A.C.M., Justino, F.B., Aguiar, R.G., da Costa, J.M.N., 2012. Modeling the photosynthetically active radiation in South West Amazonia under all sky conditions. Theor. Appl. Climatol. 108, 631–640. https://doi.org/10.1007/s00704-011-0556-z.

Alados, I., Foyo-Moreno, I., Alados-Arboledas, L., 1996. Photosynthetically active radiation: measurements and modelling. Agric. For. Meteorol. 93, 121–131. https://doi.org/10.1016/S0168-1923(98)00107-5.

Alsamamra, H., Ruiz-Arias, J.A., Pozo-Vázquez, D., Tovar-Pescador, J., 2009. A comparative study of ordinary and residual kriging techniques for mapping global solar radiation over southern Spain. Agric. For. Meteorol. 149, 1343–1357. https://doi.org/10.1016/j.agrformet.2009.03.005.

Anderegg, J., Zenkl, R., Walter, A., Hund, A., McDonald, B.A., 2023. Combining High-Resolution Imaging, Deep Learning, and Dynamic Modeling to Separate Disease and Senescence in Wheat Canopies. Plant Phenomics 5, 0053. https://doi.org/10.34133/plantphenomics.0053.

Beck, H.E., Zimmermann, N.E., McVicar, T.R., Vergopolan, N., Berg, A., Wood, E.F., 2018. Present and future köppen-geiger climate classification maps at 1-km resolution. Sci. Data 5, 1–12. https://doi.org/10.1038/sdata.2018.214.

Benavides Cesar, L., Manso Callejo, M.Á., Cira, C.-I., Alcarria, R., 2023. CyL-GHI: Global Horizontal Irradiance Dataset Containing 18 Years of Refined Data at 30-Min Granularity from 37 Stations Located in Castile and León (Spain). Data 8, 65. https://doi.org/10.3390/data8040065.

Consejería de Desarrollo Rural Ganadería Pesca Alimentación y Medio Ambiente Gobierno de Cantabria, 2022. Calidad del aire de Cantabria [WWW Document]. URL https://airecantabria.com/historico.php.

Consejo Económico y Social de Castilla y León (Ed.), 2021. Informe sobre la Situación Económica y Social de Castilla y León 2021. Tomo I. http://www.cescyl.es/es/publicaciones/informes-anuales.

de Blas, M., García-Rodríguez, A., García, I., Torres, J.L., 2022. Validation and calibration of models to estimate photosynthetically active radiation considering different time scales and sky conditions. Adv. Space Res. 70, 1737–1760. https://doi.org/10.1016/j.asr.2022.07.005.

De Kauwe, M.G., Disney, M.I., Quaife, T., Lewis, P., Williams, M., 2011. An assessment of the MODIS collection 5 leaf area index product for a region of mixed coniferous forest. Remote Sens. Environ. 115, 767–780. https://doi.org/10.1016/j.rse.2010.11.004.

Drouet, J.L., Kiniry, J.R., 2008. Does spatial arrangement of 3D plants affect light transmission and extinction coefficient within maize crops? Field Crop Res 107, 62–69. https://doi.org/10.1016/j.fcr.2007.12.015.

Dzvene, A.R., Tesfuhuney, W.A., Walker, S., Ceronio, G., 2023. Planting time and stand density effect on radiation interception and use efficiency of maize and sunn hemp intercropping in semi-arid South Africa. Agric. For. Meteorol. 341, 109690 https://doi.org/10.1016/j.agrformet.2023.109690.

Ertekin, C., Evrendilek, F., 2007. Spatio-temporal modeling of global solar radiation dynamics as a function of sunshine duration for Turkey. Agric. For. Meteorol. 145, 36–47. https://doi.org/10.1016/j.agrformet.2007.04.004.

Fang, H., Baret, F., Plummer, S., Schaepman-Strub, G., 2019. An overview of global leaf area index (LAI): Methods, products, validation, and applications. Rev. Geophys. 57, 739–799. https://doi.org/10.1029/2018RG000608.

Farré, I., Faci, J.M., 2006. Comparative response of maize (Zea mays L.) and sorghum (Sorghum bicolor L. Moench) to deficit irrigation in a Mediterranean environment. Agric Water Manag 83, 135–143. https://doi.org/10.1016/j.agwat.2005.11.001.

Foyo-Moreno, I., Alados, I., Alados-Arboledas, L., 2017. A new conventional regression model to estimate hourly photosynthetic photon flux density under all sky conditions. Int. J. Climatol. 37, 1067–1075. https://doi.org/10.1002/joc.5063.

García-Rodríguez, A., García-Rodríguez, S., Díez-Mediavilla, M., Alonso-Tristán, C., 2020. Photosynthetic active radiation, solar irradiance and the cie standard sky classification. Applied Sciences (switzerland) 10, 1–14. https://doi.org/10.3390/app10228007.

García-Rodríguez, A., Granados-López, D., García-Rodríguez, S., Díez-Mediavilla, M., Alonso-Tristán, C., 2021. Modelling photosynthetic active radiation (PAR) through meteorological indices under all sky conditions. Agric. For. Meteorol. 310, 108627 https://doi.org/10.1016/j.agrformet.2021.108627.

García-Rodríguez, A., García-Rodríguez, S., Granados-López, D., Díez-Mediavilla, M., Alonso-Tristán, C., 2022. Extension of PAR Models under Local All-Sky Conditions to Different Climatic Zones. Applied Sciences (switzerland) 12. https://doi.org/10.3390/app12052372.

Hatfield, J.L., 2014. Radiation use efficiency: Evaluation of cropping and management systems. Agron. J. 106, 1820–1827. https://doi.org/10.2134/agronj2013.0310.

Instituto Português do Mar e da Atmosfera, 2022. Clima [WWW Document]. URL https://www.ipma.pt/pt/index.html.

Instituto Tecnológico Agrario de Castilla y León Junta de Castilla y León, 2022. InfoRiego [WWW Document]. URL https://www.inforiego.org/opencms/opencms.

Instituto Tecnológico Agrario de Castilla y León, 2022. Mapa de cultivos y superficies naturales [WWW Document].

Jeong, D.I., St-Hilaire, A., Gratton, Y., Bélanger, C., Saad, C., 2017. A guideline to select an estimation model of daily global solar radiation between geostatistical interpolation and stochastic simulation approaches. Renew. Energy 103, 70–80. https://doi.org/10.1016/j.renene.2016.11.022.

Kamali, N., Khajeh Pour, M.R., Soleymani, A., 2020. Light absorption and light extinction in barley (Hordeum vulgare L.) as affected by planting dates and plant genotypes. Theor. Appl. Climatol. 142, 589–597. https://doi.org/10.1007/s00704-020-03342-w.

Kukal, M.S., Irmak, S., 2020. Light interactions, use and efficiency in row crop canopies under optimal growth conditions. Agric. For. Meteorol. 284, 107887 https://doi.org/10.1016/j.agrformet.2019.107887.

Lang, A.R.G., Yueqin, X., 1986. Estimation of leaf area index from transmission of direct sunlight in discontinuous canopies. Agric. For. Meteorol. 37, 229–243. https://doi.org/10.1016/0168-1923(86)90033-X.

Li, R., Zhao, L., Ding, Y., Wang, S., Ji, G., Xiao, Y., Liu, G., Sun, L., 2010. Monthly ratios of PAR to global solar radiation measured at northern Tibetan Plateau, China. Sol. Energy 84, 964–973. https://doi.org/10.1016/j.solener.2010.03.005.

Liu, S., Baret, F., Abichou, M., Manceau, L., Andrieu, B., Weiss, M., Martre, P., 2021b. Importance of the description of light interception in crop growth models. Plant Physiol. 186, 977–997. https://doi.org/10.1093/PLPHYS/KIAB113.

Liu, M., Mu, L., Lu, Y., Yang, H., 2021a. Forage accumulation and radiation use of alfalfa under deficit irrigation. Crop Sci. 61, 2190–2202. https://doi.org/10.1002/csc2.20480.

McCree, K.J., 1972. The action spectrum, absorptance and quantum yield of photosynthesis in crop plants. Agric. Meteorol. 9, 191–216. https://doi.org/10.1016/0002-1571(71)90022-7.

Ministerio de Agricultura Pesca y Alimentación, 2022. Sistema de Información Agroclimática para el Regadío (SiAR) [WWW Document]. URL https://eportal.mapa.gob.es/websiar/SeleccionParametrosMap.aspx?dst=1.

Ministerio de Agricultura, Pesca y Alimentación (Ed.), 2021. Encuesta sobre Superficies y Rendimientos de Cultivos en España. Resultados 2021. https://www.mapa.gob.es/es/estadistica/temas/estadisticas-agrarias/agricultura/esyrce/.

Ministerio para la Transición Ecológica y el Reto Demográfico, 2022. AEMET OpenData [WWW Document]. URL https://opendata.aemet.es/centrodedescargas/inicio.

Mizoguchi, Y., Yasuda, Y., Ohtani, Y., Watanabe, T., Kominami, Y., Yamanoi, K., 2014. A practical model to estimate photosynthetically active radiation using general meteorological elements in a temperate humid area and comparison among models. Theor. Appl. Climatol. 115, 583–589. https://doi.org/10.1007/s00704-013-0912-2.

Monsi, M., Saeki, T., 2005. On the factor light in plant communities and its importance for matter production. Ann. Bot. 95, 549–567. https://doi.org/10.1093/aob/mci052.

Myneni, R., Knyazikhin, Y., Park, T., 2015. MCD15A3H MODIS/Terra+Aqua Leaf Area Index/FPAR 4-day L4 Global 500m SIN Grid V006 [WWW Document]. NASA EOSDIS Land Processes DAAC. https://doi.org/10.5067/MODIS/MCD15A3H.006.

Nwokolo, S.C., Amadi, S.O., 2018. A global review of empirical models for estimating photosynthetically active radiation. Trends in Renewable Energy 4, 236–327. https://doi.org/10.17737/tre.2018.4.2.0079.

Nyamsi, W.W., Blanc, P., Augustine, J.A., Arola, A., Wald, L., 2019. A new clear-sky method for assessing photosynthetically active radiation at the surface level. Atmos. 10 https://doi.org/10.3390/ATMOS10040219.

Palmer, D., Cole, I., Betts, T., Gottschalg, R., 2017. Interpolating and estimating horizontal diffuse solar irradiation to provide UK-wide coverage: Selection of the best performing models. Energies 10. https://doi.org/10.3390/en10020181.

Perez, R., Ineichen, P., Seals, R., Michalsky, J., Stewart, R., 1990. Modeling daylight availability and irradiance components from direct and global irradiance. Sol. Energy 44, 271–289. https://doi.org/10.1016/0038-092X(90)90055-H.

Piccoli, F., Locatelli, S.G., Schettini, R., Napoletano, P., 2023. An open-source platform for GIS data management and analytics. Sensors 23, 3788. https://doi.org/10.3390/s23083788.

Ramirez-Garcia, J., Almendros, P., Quemada, M., 2012. Ground cover and leaf area index relationship in a grass, legume and crucifer crop. Plant Soil Environ. 58, 385–390. https://doi.org/10.17221/195/2012-pse.

Rodríguez-Amigo, M.C., Díez-Mediavilla, M., González-Peña, D., Pérez-Burgos, A., Alonso-Tristán, C., 2017. Mathematical interpolation methods for spatial estimation of global horizontal irradiation in Castilla-León, Spain: A case study. Sol. Energy 151, 14–21. https://doi.org/10.1016/j.solener.2017.05.024.

Rubio, M.A., López, G., Tovar, J., Pozo, D., Batlles, F.J., 2005. The use of satellite measurements to estimate photosynthetically active radiation. Phys. Chem. Earth 30, 159–164. https://doi.org/10.1016/j.pce.2004.08.029.

Sebastiani, A., Salvati, R., Manes, F., 2023. Comparing leaf area index estimates in a Mediterranean forest using field measurements, Landsat 8, and Sentinel-2 data. Ecol. Process. 12, 28. https://doi.org/10.1186/s13717-023-00441-0.

Sieling, K., Böttcher, U., Kage, H., 2016. Canopy traits in rye, triticale and wheat under varying N supply. Agron. Res. 14, 1467–1485.

Tabarzad, A., Ghaemi, A.A., Zand-Parsa, S., 2016. Extinction coefficients and radiation use efficiency of barley under different irrigation regimes and sowing dates. Agric Water Manag 178, 126–136. https://doi.org/10.1016/j.agwat.2016.09.020.

Tan, M., Fang, G., Stomph, T.J., Jing, W., Wen, Y., Lizhen, Z., Qiang, C., van der Werf, W., 2020. Dynamic process-based modelling of crop growth and competitive water extraction in relay strip intercropping: Model development and application to wheat-maize intercropping. Field Crop Res 246, 107613. https://doi.org/10.1016/j.fcr.2019.107613.

Tarkalson, D.D., King, B.A., Bjorneberg, D.L., Taberna, J.P., 2012. Effects of planting configuration and in-row plant spacing on photosynthetically active radiation interception for three irrigated potato cultivars. Potato Res. 55, 41–58. https://doi.org/10.1007/s11540-011-9205-2.

Tsubo, M., Walker, S., 2005. Relationships between photosynthetically active radiation and clearness index at Bloemfontein, South Africa. Theor. Appl. Climatol. 80, 17–25. https://doi.org/10.1007/s00704-004-0080-5.

Vindel, J.M., Valenzuela, R.X., Navarro, A.A., Zarzalejo, L.F., 2018. Methodology for optimizing a photosynthetically active radiation monitoring network from satellite-derived estimations: A case study over mainland Spain. Atmos. Res. 212, 227–239. https://doi.org/10.1016/j.atmosres.2018.05.010.

Wang, D., Liang, S., Zhang, Y., Gao, X., Brown, M.G.L., Jia, A., 2020. A new set of modis land products (Mcd18): Downward shortwave radiation and photosynthetically active radiation. Remote Sens. (Basel) 12. https://doi.org/10.3390/RS12010168.

Wei, S., Yin, T., Dissegna, M.A., Whittle, A.J., Ow, G.L.F., Yusof, M.L.M., Lauret, N., Gastellu-Etchegorry, J.P., 2020. An assessment study of three indirect methods for estimating leaf area density and leaf area index of individual trees. Agric. For. Meteorol. 292–293, 108101 https://doi.org/10.1016/j.agrformet.2020.108101.

Wen, H., Du, Y., Chen, X., Lim, E.G., Wen, H., Yan, K., 2023. A regional solar forecasting approach using generative adversarial networks with solar irradiance maps. Renew. Energy 216, 119043. https://doi.org/10.1016/j.renene.2023.119043.

Wojnowski, W., Wei, S., Li, W., Yin, T., Li, X.-X., Ow, G.L.F., Mohd Yusof, M.L., Whittle, A.J., 2021. Comparison of absorbed and intercepted fractions of PAR for individual trees based on radiative transfer model simulations. Remote Sens. 13, 1069. https://doi.org/10.3390/rs13061069.

Yu, L., Shang, J., Cheng, Z., Gao, Z., Wang, Z., Tian, L., Wang, D., Che, T., Jin, R., Liu, J., Dong, T., Qu, Y., 2020. Assessment of cornfield LAI retrieved from multi-source satellite data using continuous field LAI measurements based on a wireless sensor network. Remote Sens. (Basel) 12, 3304. https://doi.org/10.3390/rs12203304.

Yu, X., Wu, Z., Jiang, W., Guo, X., 2015. Predicting daily photosynthetically active radiation from global solar radiation in the Contiguous United States. Energ. Conver. Manage. 89, 71–82. https://doi.org/10.1016/j.enconman.2014.09.038.

Zhang, L., Hu, Z., Fan, J., Zhou, D., Tang, F., 2014. A meta-analysis of the canopy light extinction coefficient in terrestrial ecosystems. Frontiers of Earth Science 8, 599–609. https://doi.org/10.1007/s11707-014-0446-7.